Mathematical Modelling to Predict Nitrided Layer Thickness of Low Temperature Gas and Plasma Nitriding of AISI 316 L Stainless Steel (Austenitic)

MUHAMAD AARIF BILLAH MOHD ZULKEPLI

MECHANICAL ENGINEERING

UNIVERSITI TEKNOLOGI PETRONAS

SEPTEMBER 2013

Mathematical Modelling to Predict Nitrided Layer Thickness of Low Temperature Gas and Plasma Nitriding of AISI 316 L Stainless Steel (Austenitic)

By

MUHAMAD AARIF BILLAH MOHD ZULKEPLI

Dissertation submitted in partial requirement of

the requirements for the

Bachelor of Engineering (Hons)

(Mechanical Engineering)

SEPTEMBER 2013

Universiti Teknologi PETRONAS

Bandar Seri Iskandar

31750 Tronoh

Perak Darul Ridzuan

CERTIFICATION OF APPROVAL

Mathematical Modelling to Predict Nitrided Layer Thickness of Low Temperature Gas and Plasma Nitriding of AISI 316 L Stainless Steel (Austenitic)

By

Muhamad Aarif Billah b. Mohd Zulkepli

Project Dissertation submitted to the

Mechanical Engineering Programme

The partial fulfilment of the requirements for the

Bachelor of Engineering (Hons)

(Mechanical Engineering)

Approved by,

_____

(Mr Azman Zainuddin)

Universiti Teknologi PETRONAS

Tronoh, Perak Darul Ridzuan

September 2013

ABSTRACT

Austenitic stainless steel is one of the world most produced alloy for stainless steel production mainly due to its high corrosion resistance properties. However, austenitic stainless steel low surface hardness have always been an important issue to address. Therefore, many studies have been conducted in order to increase the surface hardness of the austenitic stainless steel without significantly affect the corrosion resistance characteristic of the stainless steel. The author's study compose only on the austenitic stainless steel type AISI 316L which is among the most produced stainless steel in the whole world.

The objective of the project is to develop a mathematical model which can provide a way for austenitic stainless steel manufacturers to predict the case depth or nitrided layer thickness of the gas and plasma nitrided austenitic stainless steel. In order to model nitrided layer growth in austenitic stainless steel with high accuracy, the author based the equation on the Fick's first law of diffusion as well the changes of microstructure phase and also the effect of austenitic stainless steel microstructure phase that is FCC. In this particular study, the author focus on the mathematical model to predict nitrided layer thickness for low temperature gas and plasma nitriding of the austenitic stainless steel in relation to the varying temperature and nitriding time.

The significant of the project to provide a working mathematical model which is able to predict the nitrided layer thickness of gas and plasma nitrided austenitic stainless steel. Therefore, the nitriding time and temperature of gas nitriding or plasma nitriding could be modelled for cost saving and efficiency in the industrial application.

In conclusion, the mathematical model is able to predict up to a good accuracy the nitrided layer thickness of the gas and plasma nitrided austenitic stainless steel of AISI 316L which can be seen in chapter 4 of the report.

CERTIFICATION OF ORIGINALITY

This is to certify that I am responsible for the work submitted in this project, that the original work is my own except as specified in the references and acknowledgements, and that the original work contained herein have not been undertaken or done by unspecified sources or persons.

_____

MUHAMAD AARIF BILLAH B. MOHD ZULKEPLI

ACKNOWLEDGEMENT

First and foremost, I would like to dedicate my special thanks to Universiti Teknologi PETRONAS for giving me the opportunity to conduct this remarkable Final Year Project (FYP) from the beginning till the completion of this project. FYP has been a great opportunity for the author to experience a large scale individual project experience in which the author learned a lot on material engineering especially in the term of diffusion mechanism in metal and alloys as well as mathematical modelling in which the author have no former experience in.

The author would also extend his gratitude to his supervisor, Mr Azman Zainuddin, who had given a lot of efforts and assistance in conducting this research as well as his cooperation and endless patience in guiding the author till the completion of the project.

In addition to Mr Azman, the author would also to acknowledge and thanks Associate Professor Dr. Patthi Hussain for his guidance especially with regards to material engineering, and most importantly with nitriding process and help for experimental data and lab works.

Other than that, the author would also like to thanks everyone who has contributed directly or indirectly in ensuring the successfulness of this Final Year Project. The help and supports are highly appreciated and very much needed in the completion of the project. Therefore, once again, the author is very grateful for the help and guidance given by all involved individuals.

Thank you.

TABLE OF CONTENTS

List of Figure

List of Table

Abbreviations

AISI : American Iron and Steel Institute

ASM : American Society for material

BCC : Body-centered cubic

FCC : Face-centered cubic

SS : Stainless steel

SCC : Stress corrosion cracking

List of Symbols and Nomenclature

ε-Fe_2N_{1-x} layer	: Nitrided layer formed, composed of thin martensitic layer, caused by gas nitriding or plasma nitriding of austenitic stainless steel which grows outward which has BCC atomic structure.
γ'-Fe_4N layer	: Nitrided layer formed, composed of expended austenitic layer, caused by gas nitriding or plasma nitriding of austenitic stainless steel which grows inward which retains the austenitic stainless steel FCC atomic structure.
Alpha (α)	: Ferritic
Gamma (γ)	: Austenitic
Gamma prime (γ')	: Expanded austenitic
epsilon (ε)	: Martensitic
C	: Concentration
t	: time
x	: Depth
D	: Diffusion coefficients
Δ	: Difference

$f(x)$	: function of x
Cr_y	: Substantially dissolved chromium
N_y	: Interstitially dissolved nitrogen in solid solution in the FCC austenitic lattice
CrN_n	: Nitrogen trapped by chromium
Ke	: Equilibrium constant for CrN_n forming reaction
K_{CrNn}	: Solubility of product of Cr_y and N_y
J_i	: Nitrogen diffusion flux, where $i = \varepsilon \; and \; \gamma' phase$
N_s	: Surface nitrogen concentration
$N_{\varepsilon/\gamma'}$	: Nitrogen concentration at interface between ε and γ' layers
$N_{\gamma'/\varepsilon}$	**:** Nitrogen concentration at interface between γ' and ε layers
λ_i	: Thickness for i layer, $i = \varepsilon \; and \; \gamma' phase$
b_i	: Constant of the growth rate
N_ε	: The nitrogen concentration distribution in ε

CHAPTER 1: INTRODUCTION

1.1 Background of Study

This project is about mathematical modelling to predict nitrided layer thickness of gas and plasma nitrided austenitic stainless steel at various low temperature gas nitriding and plasma nitriding. In this background of study section will discuss on the general information with regards to the general application of austenitic stainless steel and some information on gas and plasma nitriding as a part of surface treatment technique.

Stainless steel in general have high resistance to corrosion (rusting) in variety of environments, especially in the ambient atmosphere. Their predominant alloying element is chromium; a concentration of at least 11 wt. % is required. Corrosion resistance is also enhanced by nickel and molybdenum additions which also acts as an austenitic stabilizer. These stainless steels are divided into three classes on the basis of the predominant phase constituent of its microstructure – martensitic, ferritic and austenitic. This project however will only focus on the mathematical modelling to predict nitrided layer thickness of the AISI 316L austenitic stainless steel. Austenitic stainless steel is the most corrosion resistance type of stainless steel due to high chromium contents and nickel additions and also produced in the largest quantities worldwide. In addition, austenitic stainless steel is not a magnetic alloy like both martensitic and ferritic stainless steels.

AISI 316L is widely used in several industrial applications, mainly due to its excellent corrosion resistance; however, low hardness and poor wear performance impose strong limitation in many points. Therefore, typically a combination of DC-pulsed plasma nitriding and plasma assisted PVD coating as a surface coating have been shown to improve the material fatigue and wear resistance without affecting the corrosion performance [1] of the austenitic stainless steel which is highly appreciated. Austenitic stainless steel in particular, AISI 316L, have attracted much attention in the last years due to their excellent corrosion resistance in different environment which lead to wide application in the food and chemical processing industries as well as in biomaterial applications. As mentioned earlier, the range of possible application of austenitic stainless steel is limited by the poor hardness and low wear resistance when the application required good tribological properties.

Since the austenitic stainless steel weakness is its surface hardness and tribological properties, there is a need for a more advance surface treatment techniques in order to improve on the typical austenitic stainless steels without affecting the corrosion resistance characteristic of the material. Nitriding of austenitic stainless steels is usually characterized by the precipitation of chromium nitrides in the nitrided case, inducing precipitation hardening which is also called the 'white layer' by a mechanism term as nitrogen trapping in the form of CrN (Chromium Nitride). This leads to the depletion of chromium content in the austenitic matrix because the white layer is mainly consist of chromium oxides which lead to significant reduction in the corrosion resistance of the nitrided layer.

Over the past decade, attempts have been made to improve the corrosion resistance of nitrided austenitic stainless steels. One of these attempts involved plasma nitriding at relatively low temperatures, normally lower than 450^{o}C rather than the conventional nitriding temperature of 600 ^{o}C used for the austenitic stainless steels. This result in the production of extremely very thin layer of extremely high hardness with excellent corrosion resistance which is also observed in gas nitriding [2]. This low temperature nitrided layers produced on austenitic stainless steels were considered to be precipitation-free and composed of an uncharacterised phase (γ'). This was regarded as an expanded austenitic some as a result from super-saturation of nitrogen in the austenite.

However, there have been no previous study done in the effort to help manufacturer predict the nitrided layer thickness of the austenitic stainless steel which most regards as hard to be nitrided. According to Patthi (1997), nitrided case hardness is proportional to that of the nitrided case thickness. Therefore, if the nitrided case thickness can be model, its counterpart that is the nitrided surface hardness could be possible to model as well.

However, this project will focus on the mathematical modelling aspect in predicting the nitrided layer thickness of the austenitic stainless steel in particular AISI 316L in order to help manufacturer in determining the expected or calculated thickness of the nitrided layer of the gas nitrided or plasma nitrided austenitic stainless steel at given temperature and nitriding duration. While modelling of the relationship between the nitrided case thickness and its surface hardness value is reserved for future works.

1.2 Problem Analysis

Austenitic stainless steel is largest type of stainless steels produced in the world due to its special high corrosion resistance properties. However, austenitic stainless steels have low surface hardness and poor wear resistance which severely constricted the possible application of the austenitic stainless steel's high corrosion resistance characteristics when hardness and tribological properties is required.

The low hardness and poor wear resistance is caused by the face-centered-cubic (FCC) atomic structure which provides more planes for the flow of dislocations, combined with the low level of interstitial elements which give the material it's good ductility. However this also lead to low hardness and poor wear resistance. Among the common solution to this problem is by a combination of DC-pulsed plasma nitriding and plasma assisted PVD coating as surface treatment which have been shown to improve the material fatigue and wear resistance without affecting the corrosion performance [1] and gas nitriding or plasma nitriding of the austenitic stainless steel with lower temperature than conventional nitriding potential which create a layer of expended austenite which is very thin and very hard with minimal decrease of the corrosion resistance properties of the austenitic stainless steel by minimising the formation of chromium oxide [2].

Therefore, with respect to that gas nitriding and plasma nitriding of the austenitic stainless steel, in this project the author will try to develop a mathematical model which will be able to predict the nitrided layer thickness of the austenitic stainless steel and thus help in estimating the nitrided surface hardness value. Regardless to say, this project will only focus on the mathematical model to predict the nitrided layer thickness of AISI 316L (austenitic stainless steel).

1.3 Objectives of the Study

Objective of the study is to analyse and mathematically model the growth of nitrided layer in gas nitriding and plasma nitriding of austenitic stainless steels at low temperature nitriding and different nitriding duration in comparison to the actual experimental result from numerous sources.

1.4 Scope of the Project

The scope of the project will cover only mathematical modelling of gas nitrided and plasma nitrided austenitic stainless steel (AISI 316L) at different temperature and nitriding durations. The calculated nitrided layer thickness of the mathematical model should conform to the actual nitrided layer thickness from the experimental result. However, the mathematical model of the nitrided layer thickness would only be applicable for gas and plasma nitriding of austenitic stainless steel at low temperature (minimum temperature valid for the equation is 371^{o}C) with varying temperature and nitriding time or duration.

1.5 Significance of the Project

The mathematic model generated from the project is supposed to be able to estimate up to high accuracy the nitrided layer thickness. Therefore, the mathematical model will help the stainless steel manufacturing industry to predict the thickness of the nitrided layer prior to nitriding process and hence help to produce nitrided austenitic stainless steels desired nitrided layer thickness. This is helpful because the nitrided layer thickness is proportional to its nitrided surface hardness value.

CHAPTER 2: LITERATURE REVIEW

Nitriding is one of the technology in surface treatment engineering and one in which the author has little knowledge on. Therefore the author has conducted an extensive study and research on nitriding process, especially the gas nitriding and plasma nitriding process in relation to stainless steels and in particular, austenitic stainless steels. In addition to that, mechanical properties and microstructure of austenitic stainless steels is first studied in order to first understand the original properties of austenitic stainless steels and how it could affect the diffusion mechanism. Then this section will cover gaseous and plasma nitriding in theory and in real life and various studies that have been conducted with respect to gas nitriding and plasma nitriding mathematical modelling for pure iron.

2.1 Mechanical properties and microstructure of austenitic stainless steel

Mechanical properties describe the way that a material responds to forces, loads and impacts [12]. Austenitic stainless steels have many advantages from a metallurgical point of view. They can be made soft enough with yield strength of about 200 MPa to be easily formed by the same tools that work with carbon steel but also can be made incredibly strong by cold work for yield strength of over 2000 MPa. Their austenitic structure or rather their face-centered cubic structure is very tough and ductile down to absolute zero. In addition to that, austenitic stainless steels also do not lose their strength at elevated temperatures as rapidly as ferritic (BCC) iron based alloy. The least corrosion-resistant version of austenitic stainless steels can withstand the normal corrosive attack of the everyday environment that normal day experience while the most corrosion-resistant grades can even withstand boiling seawater.

However, these austenitic stainless steels also have weakness of their own. Austenitic stainless steels are less resistant to cyclic oxidation than are ferritic grades due to their greater thermal expansion coefficient tends to cause the protective oxide coating to spall. Austenitic stainless steels also susceptible to experience stress corrosion cracking (SCC) if used in an environment to which they have sufficient corrosion resistance. Furthermore, in comparison with ferritic stainless steels, austenitic stainless steel has fatigue endurance limit for only about 30% of the tensile strength compared to ferritic stainless steels fatigue endurance 50-60% of tensile

strength value. With this in mind, plus their high thermal expansion coefficients which make austenitic SS more susceptible to thermal fatigue [3].

The mechanical properties and chemical composition of common austenitic stainless steels [12] is as follow

Table 1 Chemical Composition of Austenitic Stainless Steel

Alloy	C	N	Cr	Ni	Mo	Mn	Si	Other	Other	Other
201	0.08	0.07	16.3	4.5	0.2	7.1	0.45	0.001S	0.03P	0.2Cu
201 drawing	0.08	0.07	16.9	5.4	0.02	7.1	0.5	0.001S	0.30P	0.6Cu
201 LN	0.02	0.13	16.3	4.5	0.2	1.0	0.45	0.001S	0.03P	0.5Cu
301 tensile	0.08	0.4	16.6	6.8	0.2	1.0	0.45	0.001S	0.03P	0.3Cu
301 drawing	0.08	0.04	17.4	7.4	0.02	1.7	0.45	0.007S	0.03P	0.6Cu
304	0.05	0.05	18.3	8.1	0.3	1.8	0.45	0.001S	0.03P	0.3Cu
304 drawing	0.05	0.04	18.4	8.6	0.3	1.8	0.45	0.001S	0.03P	0.3Cu
304 extra drawing	0.06	0.04	18.3	8.1	0.3	1.8	0.45	0.013S	0.03P	0.4Cu
304L tubing	0.02	0.09	18.3	8.1	0.3	1.8	0.45	0.013S	0.03P	0.4Ci
305	0.05	0.02	18.8	12.1	0.2	0.8	0.60	0.001S	0.02P	0.2Cu
321	0.05	0.01	17.7	9.1	0.03	1.0	0.45	0.001S	0.03P	0.4Ti
316L	0.02	0.0	16.4	10.5	2.1	1.8	0.50	0.010S	0.03P	0.4Cu

2.2 Gaseous and plasma nitriding: in theory and real life

It is common knowledge that key control parameters used to control the nitriding process and determine its outcome are temperature as well as residual ammonia or dissociation, or the more modern nitriding potential.

General rule of thumbs for gaseous nitriding which valid as long as the same material is treated:

i. Increasing the temperature will increase the case depth and increase the white layer;

ii. ii. Increasing the residual ammonia and decreasing the dissociation measured will increase the case depth and white layer; and

iii. Increasing the nitriding potential will increase the case depth and white layer.

As according to point (i) temperature is without a doubt an important influence in nitriding and all other case hardening treatments. At higher temperatures the iron lattice provides more space for nitrogen atoms to diffuse further into the metal part. Typical nitriding processes are carried out between 495-565^{O}C. Beyond this temperature limit or range, interstitial diffusion of nitrogen atoms occurs. Some scientist refers to it as high temperature gas nitriding while others like Winter (2009) suggest that such mechanism is not gas nitriding where he argued that such process is more similar to carburizing where the carbon is replaced by nitrogen [12].

As according point (ii) to control the atmosphere conditions, the measuring equipment used must be known. An ammonia analysers would be very useful in calculating the ammonia percentage in the furnace, but readings are actually taken of the residual ammonia in the exhaust. With a burette or a hydrogen analyser, the dissociation rate is based on the percentage of all gases except ammonia in the exhaust. Therefore, point (ii) of the rule thumb hold true where the more ammonia the higher the nitriding effect.

On the other hand, plasma or ion nitriding process is based on the familiar chemistry of gas nitriding, which uses a plasma discharge of reaction gases both to heat the steel surface and to supply nitrogen ions for nitriding. The process dates back to the work of a German physicist, Dr. Wehnheldt, who in 1932 developed what he called the “glow discharge” method of nitriding. Wehnheldt encounter severe problems with the control of the glow discharge. He then partnered with a Swiss physicist and entrepreneur, Dr. Bernhard Berghaus. Together they stabiled the process and later formed the company Klockner Ionen GmbH, specializing in the manufacture of ion nitriding equipment. Although the ion nitriding process developed by Wehnheldt and Berghaus was used successfully by German industrialist during World War II, it was not used extensively because it was considered too complex, too expensive and too unreliable to guarantee consistent and repeatable results. Not until the 1970s did the process gain industrial acceptance, particularly in Europe.

The significant of the glow discharge process was that it did not rely on the decomposition or cracking of a gas to liberate nascent nitrogen on the steel surface. The process was based on the ionization of a single molecular gas, which is nitrogen

and the liberation of nitrogen ions. The process offered a shorter time cycle due to the steel surface preparation and the gas ionization [3].

2.3 Nitrided growth layer of austenitic stainless steel

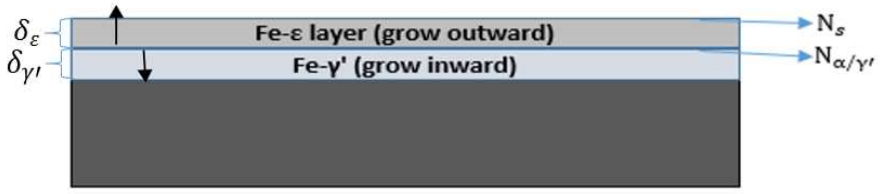

Figure 2.1 the nitride growth structure formed on the austenitic stainless steel

The nitrided layer form on the surface of the austenitic stainless steel can be observed as in Figure 2.1. The nitrided specimens were section perpendicularly to the surface and according to Billion and Hendry (1985), this change is the result of nucleation and growth of ε-Fe_2N_{1-x}, which forms on the origin metal surface and grows outward while the subsurface layer of γ'-Fe_4N grows inwards. This is very important which lead the author to the equation to predict the nitrided layer growth in austenitic stainless steels.

The microstructure phase of the austenitic stainless steel which is FCC also plays an important role in predicting the estimated thickness of nitrided layer growth in the gas and plasma nitrided austenitic stainless steels.

According to chapter 6 of ASM International Handbook (2008), there are a special relationship between martensite and austenite phase which mainly involved due to stability effect. This entails that formation of martensite on the surface of austenite stainless steel at room temperature maybe thermodynamically possible, but the driving force for its formation may be insufficient for it to form spontaneously. However, since martensite form from unstable austenite by a diffusion less shear mechanism, it can occur if that shear is provided mechanically by external forces.

2.4 Nitrogen diffusion and nitrogen depth profiles in expanded austenite: experimental assessment, numerical simulation and role of stress by T. Christiansen, K.V. Dahl and M.A.J. Somers.

The present paper addresses the experimental assessment of the concentration dependent nitrogen diffusion coefficient in stress free expended austenitic foils from thermogravimetry, the numerical simulation of nitrogen concentration depth profiles

on growth of expended austenite into stainless steel during gaseous nitriding, a qualitative discussion of the role of stress on local equilibrium conditions of growing expanded austenite and a discussion of the erroneous concentration dependent diffusivity of nitrogen in expended austenite as obtained from applying the Boltzmann-Matano method to composition-depth profiles.

2.4.1 Modelling: Simulation of nitrogen diffusion depth profiles (nitrided ferritic alloy)

A numerical model for the prediction of nitrogen concentration profile in nitrided ferritic alloys containing nitride forming elements was developed by Sun and Bell [13] based on explicit finite difference method. The nitrogen content present in precipitated alloying element nitride (e.g. CrN) was accounted for by incorporating the thermodynamic solubility constant K_e of the pertinent precipitation reaction. Recently, modifications of the Sun and Bell model have been proposed by Schacherl et al. [14] and by Kammingga and Janssen [15] for ferritic nitriding. In all the above mentioned simulations of nitrogen concentration profiles, the diffusion coefficient of nitrogen in ferrite was considered independent of the nitrogen content. Furthermore, these models represent (at least) two phase systems where nitrides are dispersed in a ferritic matrix. None of the models presented so far takes the effects of nitride dispersion on nitrogen diffusion into consideration.

In this paper, a modified version of the model used in [13] and [14] is applied and adopted to the case interstitial diffusion in austenitic stainless steel and the associated development of nitrogen stabilised expended austenite γ_N where no precipitation of nitrides occurs. This system is a continuous, single phase system, because the transition from expended austenite to the austenite bulk is accomplished by the dissolution of nitrogen into the austenite lattice. As compared to diffusion of nitrogen in ferrite, it is essential to incorporate the concentration dependence of the diffusivity of nitrogen.

The model are as follows which was developed based on the Fick's second law of diffusion:

$$\frac{\partial C(x,t)}{\partial t} = \frac{\partial}{\partial x}\left[D(C)\frac{\partial C(x,t)}{\partial x}\right] \ldots . eqn\ (1)$$

Where D(C) is the concentration dependent diffusion coefficient of nitrogen, *x* is the depth, *t* is the time and C (x, t) is the nitrogen concentration at depth x for time t.

To solve the differential equation, a numerical finite difference method can be applied which uses a uniform one-dimensional mesh where the geometry to be modelled is split into N nodes or grid points separated by Δx. Therefore, by applying finite difference approximations [16], the equation 1 can be discretised to

$$\frac{C_i^{t+\Delta t} - C_i^t}{\Delta t} = \frac{D_{i+1}^t - D_{i-1}^t}{2\Delta x} \cdot \frac{C_{i+1}^t - C_{i-1}^t}{2\Delta x} + D_i^t \frac{C_{i+1}^t - 2C_i^t + C_{i-1}^t}{(\Delta x)^2} \ldots eqn\ (2a)$$

Where the subscript *I* denotes the node number and Δt is the time step. Simple rewriting of equation (2a) allows for calculation of the nitrogen concentration in the node point *i* from concentrations prescribed at the previous time steps

$$C_i^{t+\Delta t} = \left(\frac{D_{i+1}^t - D_{i-1}^t}{2\Delta x} \cdot \frac{C_{i+1}^t - C_{i-1}^t}{2\Delta x} + D_i^t \frac{C_{i+1}^t - 2C_i^t + C_{i-1}^t}{(\Delta x)^2} \right) \Delta t + C_i^t \ldots eqn\ (2b)$$

The forward Euler formulation in equation (2b) is explicit in nature and therefore, a stability criterion of $\Delta t \leq \Delta x^2/2D$ must be obeyed to avoid instabilities in the calculated profiles. Thus by progressing in time, the nitrogen profile can be calculated for a given set of boundary conditions.

At the outer boundary located at the surface, the concentration C_S is presumed either constant (as per equation (3a)) or as a function of time (as per equation (3b))

$$\frac{\partial C_S}{\partial t} = 0;\ C_{i=0} = constant \ldots eqn\ (3a)$$

$$C_{i=0} = f(t) \ldots eqn\ (3b)$$

Where *f (t)* is a function of time, which can take different forms. For symmetry reasons, only half the thickness of the specimen has to be considered. To have a model that applies both for semi-finite (bulk specimens) and finite systems (thin foils), a zero flux boundary is assigned to last node point, corresponding to the mid plane of the specimen. Effectively, it is therefore possible to simulate through nitriding where the symmetrical nitrogen profiles coincide at the centre of the sample. For all simulations, an equidistant grid was applied with a spacing of 0.1 µm between successive grid points.

In addition to interstitial diffusion of nitrogen into the alloy, nitrogen trapping is also considered. The trapping of nitrogen by chromium can formally be described as

$$Cr_\gamma + nN_\gamma \rightarrow CrN_n \ \ldots eqn\ (4)$$

Where Cr_y and N_y denote substitutionally dissolved chromium and interstitially dissolved nitrogen in solid solution in the FCC austenite lattice, CrN_n denotes nitrogen trapped by chromium, which most probably can be attributed to short range ordering of N and Cr. The equilibrium constant of reaction of equation 4 is given by

$$K_e = \frac{1}{[Cr_\gamma][N_\gamma]^n} = \frac{1}{K_{CrN_n}} \rightarrow K_{CrN_n} = [Cr_\gamma][N_\gamma]^n \ldots eqn\ (5)$$

Where the square brackets denotes concentrations of the dissolved elements and K_{CrNn} is the solubility product of Cr_y and N_y.

However, the applied surface concentration C_S in the simulation is not equal to the total surface concentration because trapping, as described by the solubility product, will raise the total concentration. Consequently, when the value of the solubility product is changed, the total (surface) nitrogen concentration also changes for a constant value of C_S. In the present calculations, the total surface nitrogen concentration was kept constant which implies C_S is allowed to vary when K_{CrNn} is set to different values.

2.5 Calculation and experimentation of the compound layer thickness in gas and plasma nitriding of iron by S.R. Hosseini, F.Ashrafizadeh, and A. Kermanpur.

In the study, the thickness of compound layers formed on the surface of pure iron during the nitriding process was analytically calculated and compared with experimental data in the gaseous and plasma nitriding. Plasma nitriding was carried out on a high purity iron substrate at a temperature of 550^{o}C in an atmosphere of 75 vol. % H_2 and 25 vol. % N_2 for various nitriding times. The thickness of compound layers was evaluated by several characterization techniques including optical microscopy, SEM and XRD. Using the Fick's first diffusion law and a mass conservation rule, two separate equations were developed for predicting the thickness of the binary compound layers; epsilon (ε) and gamma prime (γ'), in terms of the nitriding process parameters. The result of the modelling indicated a good agreement with experimental data, provided appropriate correlation factors are applied. The

flexibility and reliability of the models were increased by introducing two factors, K_{ε} and $K_{\gamma'}$; the calculated curves corresponded well with both gaseous and plasma nitriding experimental data.

2.5.1 Formation of compound layers

The solubility of nitrogen in iron at room temperature is very limited but increases as the temperature increases and reaches at a maximum of 0.4 at% (0.1 wt %) at 592°C. In the nitriding process of iron, when the nitrogen concentration exceeds the solubility, extra nitrogen atoms make stoichiometric compounds with iron atoms, therefore, precipitating intermediate iron nitrides. The surface composition of the nitrided iron can be predicted by considering the Fe-N binary phase diagram. Based on the Figure 2.2, several phases and compounds including alpha (α), gamma (γ), gamma prime (γ'), epsilon (ε), zeta (ξ) etc. may theoretically be formed during the nitriding process.

As the nitrogen potential on the surface of the components does not commonly exceed 10 wt% some of the phases present in the equilibrium diagram, for example ξ and nitrogen rich compounds, cannot be formed during the nitriding process. therefore, the surface structure of the nitrided iron generally includes α-Fe(N) diffusion zone (solid solution of nitrogen in α-Fe), γ' and ε compound layers. The γ' nitride phase is an intermediate compound with a stoichiometry close to Fe_4N with 20 at% (5.9 wt %) nitrogen. The ε nitride is an intermediate phase that is formed in a range of nitrogen concentration, thus, it is generally demonstrated as $Fe_{2-3}N$. Theoretically, the maximum solubility of nitrogen in the ε phase is about 33 at% (11 wt %), but according to the nitrogen activity in the actual nitriding process, the nitrogen concentration in the ε nitride phase does not generally exceed 9 wt%. The nitrogen concentration in ε, γ' and α diffusion zone are schematically demonstrated in Figure 2.2 below.

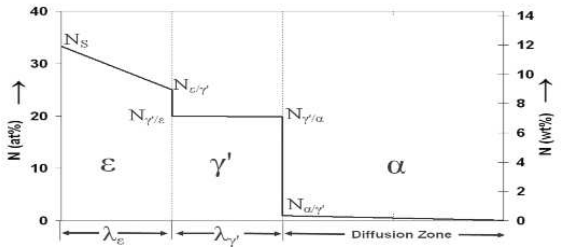

Figure 2.2. Prediction of nitrogen distribution in layers that can be formed on the surface of nitrided iron

According to S.R. Hosseini et al. a model that takes into account actual parameters of nitriding process, in the present works which generated the equation below:

$$\delta_{\varepsilon} = K_{\varepsilon} b_{\varepsilon} \sqrt{t} = K_{\varepsilon} \sqrt{\left(4D_{\varepsilon} - 0.2D_{\gamma'}\right)t} \ldots eqn\ (6)$$

$$\delta_{\gamma'} = K_{\gamma'} \left[\sqrt{(b_{\varepsilon} + 0.02\sqrt{D_{\alpha}})^2} - \left(b_{\varepsilon} + 0.02\sqrt{D_{\alpha}}\right) \right] \sqrt{t} \ldots eqn\ (7)$$

Where δ_{ε} and $\delta_{\gamma'}$ are corrected thickness of ε and γ' nitride layers, Kε and Kγ' will be changed, e.g. decreasing the surface concentration, Kε approaches zero.

Figure 2.3 shows the thickness of ε nitride versus Kε and the nitriding time at constant nitriding temperature, 550°C. Thickness of γ' nitride layer versus Kγ' and nitriding time at constant nitriding temperature 550°C are presented in Figure 2.4. It can be concluded that, at any given K, the growth rate of each layer is high at the primary stages of the nitriding process, but it decreases rapidly after about 1-3 hours. This phenomenon can be explained by considering the parabolic growth rate. Moreover, the thickness of both ε and γ' layers increases rapidly with increasing Kε and Kγ' respectively.

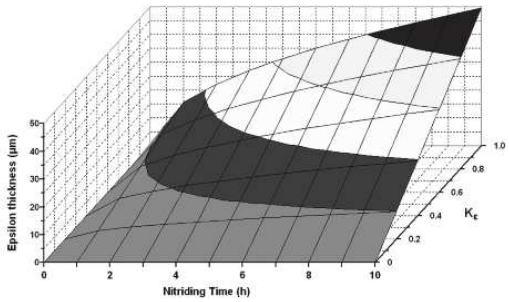

Figure 2.3. Thickness of epsilon nitride versus Kε and nitriding time at constant nitriding temperature, 550°C, in three dimensional scales

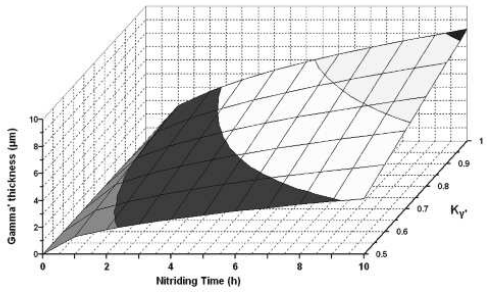

Figure 2.4. Thickness of gamma prime nitride versus Kγ' and nitriding time at constant nitriding temperature, 550^{o}C, in three dimensional scales.

For evaluation of the reliability of the above models, the thickness of ε and γ' layers at several given Kε and Kγ' were calculated and compared with the experimental data of the present work along with data obtained from the literature review [17,18,19,20]. Figure 2.5 shows the calculated thickness of ε and γ' layers versus nitriding time at 570^{o}C with Kε = 0.3 and Kγ' = 0.6, respectively, and compared with data reported by Somers and Mittemeijer in the gas nitriding process [17]. They used a gas mixture of NH_3-H_2 with 56.1 vol. % NH_3 (r_N = 6.06 x E-3 Pa-1) and good agreement is observed between their experimental data and the purposed model.

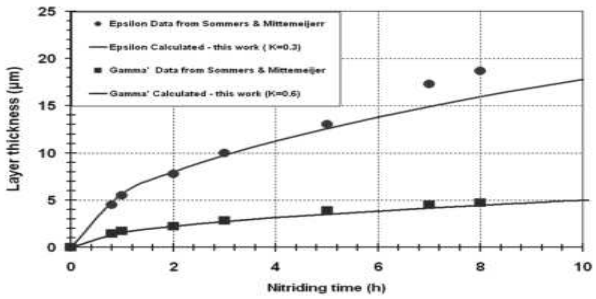

Figure 2.5. Thickness of ε and γ' layers versus nitriding time at 570^{o}C calculated in this work, compared with data from Somers and Mittemeijer [17].

Thickness of ε and γ' layers at a temperature of 575^{o}C were calculated at Kε = 0.2 and Kγ' = 0.5, respectively, and compared with data reported by Du and Agren [18] as demonstrated in Figure 2.6. their experimental findings in the gas nitriding process with nitrogen surface content of 8 wt%, evidenced that the result of the present modelling correspond very well with these data.

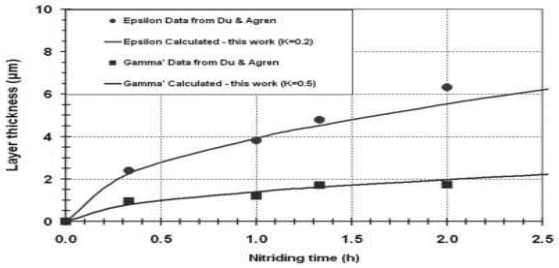

Figure 2.6 thickness of ε and γ' layers at 575^{o}C calculated in the work compared with data from Du and Agreen [18]

Figure 2.7 shows the thickness of ε and γ' layers versus nitriding time at a temperature of 570^{o}C calculated with Kε=0.2 and Kγ'=1.7, respectively, and compared with data published by Torchane, et al [19]. Their experiments were performed under the condition of gas nitriding in a mixture of NH_3-N_2-H_2 with a nitrogen surface content of 8.5 wt%. It is clear that the results of the current model correspond very well with the experimental data.

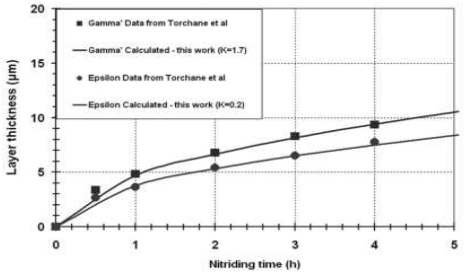

Figure 2.7. Thickness of ε and γ' layers versus nitriding time at 570^{o}C calculated in this work, compared with data from Torchane et al [19].

In conclusion, the correlation factors, Kε and Kγ' introduced in this work, increased the flexibility and reliability of the models, therefore, the calculated data corresponded very well with the experimental data in several gas and plasma nitriding conditions. In practical nitriding conditions, it would be possible to find Kε and Kγ' by carrying out a few experiments and then, predicts thickness of the compound layers under any nitriding cycle.

CHAPTER 3: METHODOLOGY

Methodology section will present the procedure that the author used in order to complete the study and as well as the project flow charts as in the Figure 3.1 and also gantt chart which covers both FYP I and II.

3.1 Overall Project Flow Chart

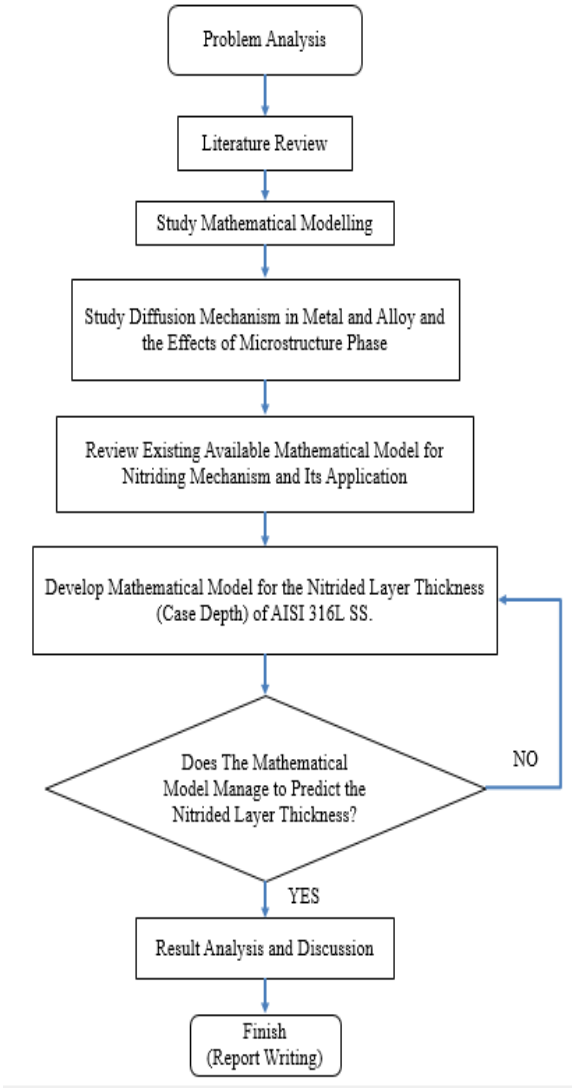

(1) Problem Analysis: Define and set parameters applicable for the problem statement.

(2) Literature Review: Cover all the essential aspect of mathematical modelling, diffusion mechanism and gas and plasma nitriding process.

(3) Review Existing Available Mathematical Model: Review whether the mathematical equation are applicable for the gas nitrided austenitic stainless steel at the set parameter.

(4) Develop Mathematical Model for Predicting Nitrided Layer Thickness for AISI 316L: The mathematical model developed is depth as a function of time.

(5) Check whether the model comply with the experimental data: If the mathematical model does not comply with experimental data, re-do the equation.

(6) Result and Discussion: Analysis the result of the equation developed against experimental data.

Figure 3.1 final Year Project (I & II) Flow Chart

3.2 Methodology for Mathematical Modelling

A mathematical model can be broadly defined as a formulation or equation that expresses the essential features of a physical system or process in mathematical terms. In a very general sense, it can be represented as a functional relationship of the form

$$Dependent\ Variable = f(indepedent\ variable, parameters, forcing\ functions)$$

Where the dependent variable is a characteristic that usually reflects the behaviour or state of the system; the independent variables are usually dimensions, such as time and space, along which the system's behaviour is being determined; the parameters are reflective of the system's properties or composition; and the forcing functions are external influences acting upon it.

The process flowchart in developing the mathematical modelling of nitrided layer growth in austenitic stainless steel is represented in Figure 3.2.

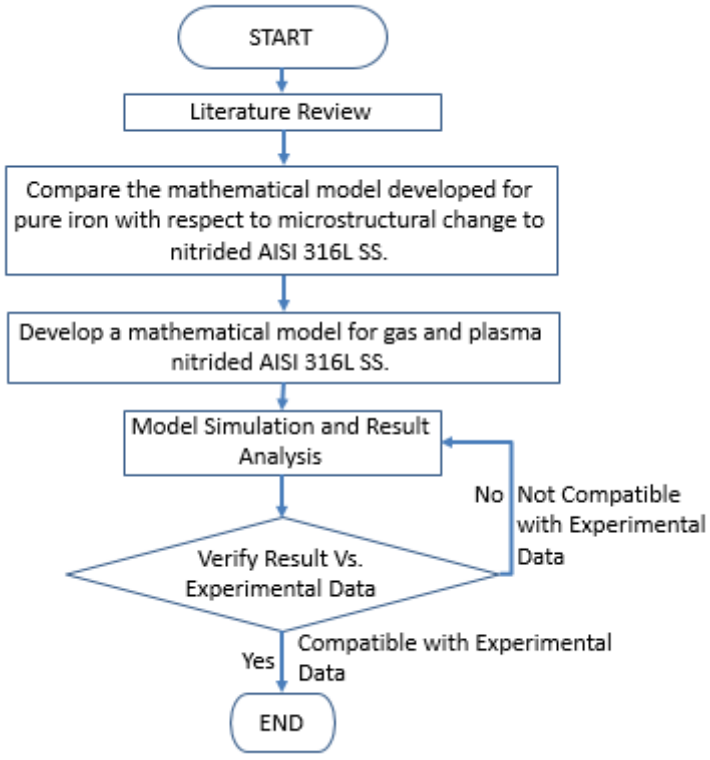

Figure 3.2. Mathematical modelling process flowchart

The mathematical model was developed by studying the model developed for the gas nitriding and plasma nitriding of pure iron by Hosseini et al (2007). After that, the model was manipulate to resemble the diffusion mechanism of gas and plasma nitriding of austenitic stainless steel. The mathematical model is then tested with different nitriding temperature and time based on experimental data gathered from various sources to see whether the mathematical model manage to predict the nitrided layer thickness of the gas nitrided or plasma nitrided austenitic stainless steel. If the mathematical model failed to predict the nitrided layer thickness, the whole steps is re-do in order to develop a more accurate mathematical model.

3.3 Softwares required for the Project (as per table 3.1)

Table 3.1 Software required by the project

Mathematical Modelling	Excel, Matlab, and Sigma plot.

3.4 Project Gantt-chart and Key Milestones

A gantt chart is a type of bar chart that is widely used to illustrate a project schedule by indicating the start and finish dates of the terminal elements and summary elements of a project. The author's project works projection is displayed in the Gantt chart shown in the next page on figure 3.3.

FYP I&II Gantt Chart

Period Highlight: 32 Plan

	ACTIVITY	PLAN START	PLAN DURATION	PERCENT COMPLETE
(1)	Chose possible project titles	1	1	100%
(2)	Study project titles in interest	2	1	100%
(3)	Preliminary Research on the titles	2	1	100%
(4)	Finalised chosen topic	2	1	100%
(5)	Problem statement analysis	2	2	100%
(6)	Extensive literature review	4	3	100%
(7)	Extended proposal submission	4	5	100%
(8)	Request for Quotation & buy speciment	5	1	100%
(9)	Interim report draft & writing	9	8	100%
(10)	Interim report submission	16	1	100%
(11)	Specimen Preparation	17	1	100%
(12)	Lab works (LOM)	17	5	80%
(13)	Review available mathematical models	21	3	100%
(14)	Study the effect of microstructure phase on the diffusion mechanism	21	3	100%
(15)	Study the microstructure of austenitic stainless steel	21	3	100%
(16)	Developing the mathematical model (s) of nitride layer growth	23	5	80%
(17)	Check the mathematical result with the experimental data	24	5	80%
(18)	Generate a curve fitting of the experiment data range	28	4	0%
(19)	Result analysis and discussion	31	5	80%
(20)	Documentation of the project	8	27	75%
	TOTAL TIME NEEDED	1	34	75%

PERIODS (WEEK)

May-13 | Jun-13 | Jul-13 | Aug-13 | Sep-13 | Oct-13 | Nov-13 | Dec-13 | Jan-14

1 2 3 4 5 6 7 8 9 10 11 12 13 14 15 16 17 18 19 20 21 22 23 24 25 26 27 28 29 30 31 32 33 34

Figure 3.3 the Project Gantt chart

CHAPTER 4: RESULT & DISCUSSION: MATHEMATICAL MODEL OF NITRIDED LAYER GROWTH IN AUSTENITIC STAINLESS STEEL

In this particular section, the author will descript on how the mathematical model was develop by briefly going through the basic process in coming up with the model which include defining the elements for the mathematical model, describing the growth kinetics of the nitride layer, then the model itself and finally the comparison between the estimated result from the mathematical model and the experimental result from various sources.

This chapter is organized by firs defining and explaining the derivation of the mathematical model which is followed by the mathematical calculation of the estimated thickness of various temperature and nitriding time as per experimental parameter conducted by numerous individuals. Later on, the mathematical calculation result is to be compared with the actual experimental results where the accuracy and limitation of the equation is discussed and scrutinize by the author.

4.1 Defining the elements for the mathematical model

In order to develop a mathematical model, all the independent variables, parameters and forcing functions are established since a mathematical model are descript as the equation below.

$$Dependent\ Variable = f(indepedent\ variable, parameters, forcing\ functions)$$

Therefore it is important to define these elements first prior to actually developing a mathematical equation. The definition of each elements are as per table 4.1.

Table 4.1. Defining the elements in the mathematical model

Equation Elements	**Definition(s)**		
Dependent Variable	Nitrided layer thickness below surface of the austenitic stainless steel.		
Independent Variable	Nitriding Time : Hour(s)		
Parameters	Gas Flow rate	N	$cm^3 . min^{-1}$ or %
		H_2	$cm^3 . min^{-1}$ or %
		NH_3	$cm^3 . min^{-1}$ or %
Forcing Parameter	Nitriding temperature		

4.2 Description on the growth kinetics of the nitride layer

The nitrided layer form below the surface of the austenitic stainless steel are observed as in Figure 2.1. The nitrided specimens were section perpendicularly to the surface and according to Billion and Hendry (1985), this change is the result of nucleation and growth of ε-Fe_2N_{1-x}, which forms on the origin metal surface and grows outward while the subsurface layer of γ'-Fe_4N grows inwards. This is very important which lead the author to the equation to predict the nitrided layer growth in austenitic stainless steels [24].

The microstructure phase of the austenitic stainless steel which is FCC also plays an important role in predicting the estimated thickness of nitrided layer growth in the gas nitrided austenitic stainless steels. For stability of the microstructure, it is possible that formation of martensite at room temperature may be thermodynamically possible which lead to the formation of ε-Fe_2N_{1-x} which must be considered in the mathematical modelling of the diffusion model.

Since according to chapter 6 of ASM International Handbook (2008), there are a special relationship between martensite and austenite phase which mainly involved due to stability effect. This entails that formation of martensite on the surface of austenite stainless steel at room temperature maybe thermodynamically possible, but the driving force (as mentioned earlier in this section is the temperature) for its formation may be insufficient for it to form spontaneously. However, since martensite form from unstable austenite by a diffusion less shear mechanism, it can occur if that shear is provided mechanically by external forces or an increase in the driving force (temperature) up to that significantly higher than the room temperature. Granted that the project entitle, mathematical modelling of nitride layer growth in gas nitrided austenitic stainless steels at low temperature, but these low temperature for gas and plasma nitriding process is significantly higher than that of the room temperature.

Therefore, based on the arguments presented, the author considered the formation of ε-Fe_2N_{1-x} which grows outward alongside with the formation of γ'-Fe_4N which grows inwards for a much more precise and conclusive mathematical model to predicts the thickness of the nitrided layer or also can be termed as the thickness of the nitrogen diffusion.

4.3 The mathematic model of nitrided layer growth in gas nitrided austenitic stainless steel.

The mathematic model will make use primarily in the Fick's first law for the nitriding process which can be expressed as equation (4.1)

$$J_i = -D_i \frac{\partial N_i(x,t)}{\partial x} \text{ , where } i = \varepsilon \text{ and } \gamma' \text{phase} \ldots eqn\ (4.1)$$

Therefore, the Fick's first law for nitrogen diffusion in each phase yields the following expression:

$$J_\varepsilon = -D_\varepsilon \frac{\partial N_\varepsilon(x,t)}{\partial x} \ldots eqn\ (4.2)$$

$$J_{\gamma'} = -D_{\gamma'} \frac{\partial N_{\gamma'}(x,t)}{\partial x} \ldots eqn\ (4.3)$$

Where J_ε and $J_{\gamma'}$ are nitrogen fluxes, D_ε and $D_{\gamma'}$ are the diffusion coefficients of nitrogen, and N_ε and $N_{\gamma'}$ are nitrogen concentrations in the ε and γ' phases respectively.

The surface nitrogen concentration can be calculated from the following equation (4.3)

$$N_s = 12.3 \exp\left(\frac{-4176}{T}\right) \ldots [wt\%] \ldots eqn\ (4.3)$$

The mass conservation rule for the compound layers can be used in common with other investigation [21, 22] indicate the results which is expressed in the following equation (4.4).

$$W_\varepsilon \frac{d\varepsilon}{dt} = [J_\varepsilon - J_{\gamma'}]_{X=\lambda\varepsilon} \ldots eqn\ (4.4)$$

Since the actual concentration are unknown, the following assumption of equilibrium is taken as per Fe-N system (as per pure iron in Figure2.3) since Fe is the main element in the austenitic stainless steel alloy, and also the initial and boundary conditions can be expressed as per the following:

I. Maximum concentration of nitrogen in ε-$Fe_{2\text{-}3}N$ nitrides reaches 11.14 wt%, when it is assumed as Fe_2N with a nitrogen content of 33.33 at%. The concentration of nitrogen in ε-$Fe_{2\text{-}3}N$ nitride decrease to a minimum value of

7.71 wt% near the γ' interface, when it is assumed as Fe_3N including 25.0 at% N.

II. Concentration of nitrogen in γ' nitride is approximately equal to 5.9 wt%, assuming to be the stoichiometric compound of Fe_4N with 20 at% N. according to the data from literature [21], it is in the range of 5.76 to 5.90 wt%.

Therefore by considering the boundary conditions I and II, and referring to Figure 2.3, the nitrogen concentration at interfaces between the ε and γ' layers can be expressed as the following equation (4.5) and equation (4.6).

$$\boldsymbol{N_{\varepsilon/\gamma'} \approx 7.71\ wt\%\ \ldots eqn\ (4.5)}$$

$$\boldsymbol{N_{\gamma'/\varepsilon} \approx 5.91\ wt\%\ \ldots eqn\ (4.6)}$$

On the other hand, the growth of compound layers follows a parabolic law which is expressed as

$$\lambda_i = b_i\sqrt{t}$$

where λ_i, b_i and t are the thickness of i layer, the constant of the growth rate and the nitriding time respectively. Therefore at a constant temperature for ε and γ' layers are

$$\lambda_\varepsilon = b_\varepsilon\sqrt{t}\ \ldots eqn\ (4.7)$$

$$\lambda_{\gamma'} = b_{\gamma'}\sqrt{t}\ \ldots eqn\ (4.8)$$

where b_ε and $b_{\gamma'}$ are constants of the growth rate. Derivation of the above equation would lead to these following equations:

$$\frac{d\lambda_\varepsilon}{dt} = \frac{b_\varepsilon}{2\sqrt{t}}\ldots eqn\ (4.9)$$

$$\frac{d\lambda_{\gamma'}}{dt} = \frac{b_{\gamma'}}{2\sqrt{t}}\ldots eqn\ (4.10)$$

4.3.1 Calculating the ε-$Fe_{2\text{-}3}N$ layer thickness

Therefore by taking into account equations (4.4), (4.7), (4.8), and (4.9) can be arranged as

$$\frac{0.9b_\varepsilon}{\sqrt{t}} = [J_\varepsilon - J_{\gamma'}]_{x=\lambda\varepsilon}\ \ldots eqn\ (4.11)$$

The nitrogen concentration distribution in ε, calculated in the literature [23] and developed to the equation (4.12)

$$N_\varepsilon = N_S + \frac{7.712 - N_S}{\text{erf}(\frac{\lambda_\varepsilon}{2\sqrt{tD_\varepsilon}})}\text{erf}\left(\frac{x}{2\sqrt{tD_\varepsilon}}\right) \dots eqn\ (4.12)$$

Where N_S is the nitrogen concentration at the surface of the work piece as demonstrated in Figure 2.3 Derivation and simplification of the above equation yields nitrogen flux at the interface between the ε and γ' nitride as equation (4.13)

$$J_\varepsilon|_{x=\lambda\varepsilon} \approx 3.4\ \frac{D_\varepsilon}{\lambda_\varepsilon} \dots eqn\ (4.13)$$

On the other hand, nitrogen concentration distribution in γ' layer can be calculated by the equation (4.14) and yield nitrogen flux of equation (4.15) [23].

$$N_{\gamma'} = \frac{0.14\lambda_\varepsilon + 5.9\lambda_{\gamma'}}{\lambda_{\gamma'}} - \frac{0.28\sqrt{TD_{\gamma'}}}{\lambda_{\gamma'}}\text{erf}\left(\frac{x}{2\sqrt{tD_{\gamma'}}}\right) \dots eqn(4.14)$$

$$J_{\gamma'} = 0.14\frac{D_{\gamma'}}{\lambda_{\gamma'}} \dots eqn\ (4.15)$$

By replacing equations (4.13) and (4.14) into (4.11), the constant of the ε nitride growth rate,b_ε , and thus the thickness of the ε layer can be calculated versus time and diffusion coefficient as represented in equation (4.16) and (4.17).

$$b_\varepsilon \approx \sqrt{4D_\varepsilon - 0.2D_{\gamma'}} \dots eqn\ (4.16)$$

$$\lambda_\varepsilon \approx \sqrt{\left(4D_\varepsilon - 0.2D_{\gamma'}\right)t} \dots eqn\ (4.17)$$

4.3.2 Calculation of γ' nitride thickness

For the calculation of γ' nitride thickness, we take into the consideration the nitrogen concentration on the surface as per equation (4.3). Same process as per calculation of ε-$Fe_{2\text{-}3}N$ layer which yield the following equation.

$$b_{\gamma'} \approx 0.5\left[-\left(b_\varepsilon + 0.02\sqrt{D_\alpha}\right) + \sqrt{\left(b_\varepsilon + 0.02\sqrt{D_\alpha}\right)^2 + 0.2D_{\gamma'}}\right] \dots eqn\ (4.18)$$

$$\lambda_{\gamma'} \approx 0.5\left[-\left(b_\varepsilon + 0.02\sqrt{D_\alpha}\right) + \sqrt{\left(b_\varepsilon + 0.02\sqrt{D_\alpha}\right)^2 + 0.2D_{\gamma'}}\right] \cdot \sqrt{t} \dots eqn\ (4.19)$$

4.3.3 Calculating the diffusion coefficients

$$D_{\varepsilon} = 2.1 \times 10^{-8} \exp[\frac{-93517 \frac{J}{mol}}{8.314T \cdot \frac{J}{mol \cdot K}}]$$

$$D_{\gamma'} = 1.7 \times 10^{-9} \exp[\frac{-64000 \frac{J}{mol}}{8.314T \cdot \frac{J}{mol \cdot K}}]$$

$$D_{\alpha} = 6.6 \times 10^{-7} \exp[\frac{-77900 \frac{J}{mol}}{8.314T \cdot \frac{J}{mol \cdot K}}]$$

4.4 Conclusion for the mathematical model

As mentioned earlier, the total nitrided layer growth mathematical model of austenitic stainless steel must account for the γ' nitride thickness and ε-Fe2-3N layer thickness. Therefore, the total thickness of the nitrided layer growth below the surface is the addition of γ' nitride thickness and ε-Fe2-3N layer thickness.

$$Total\ thickness\ for\ the\ nitrided\ layer\ growth\ = \lambda_{\gamma'} + \lambda_{\varepsilon}$$

$$\lambda_{\gamma'} \approx 0.5\left[-\left(b_{\varepsilon} + 0.02\sqrt{D_{\alpha}}\right) + \sqrt{\left(b_{\varepsilon} + 0.02\sqrt{D_{\alpha}}\right)^2 + 0.2D_{\gamma'}}\right] \cdot \sqrt{t} \ldots eqn\ (4.19)$$

$$\lambda_{\varepsilon} \approx \sqrt{\left(4D_{\varepsilon} - 0.2D_{\gamma'}\right)t} \ldots eqn\ (4.17)$$

4.5 Gas Nitriding: Calculation result for 600°C in comparison to Patthi (1997) for AISI 316L SS [24]

Table 4.51 below indicates the experimental parameter details from the reference [24]. The experiment were carried out to investigate the thickness of the nitrided layer after 2, 24 and 48 hours of gas nitriding. The material used for the experiment are AISI 316L SS plates. The experiment is a single stage gas nitriding process where the nitriding process is done at a single nitriding temperature, in this case 600°C.

Table 4.5.1 Experimental details for Patthi 316L nitriding at 600°C

Experimental Details					
Time	[0 2 24 48] Hour(s)		**Nitrogen Flow rate**	200	cm^3*min-1
Temperature	873	Kelvin	**GM H2**	100	cm^3*min-1
Sample Size	12.9 mm X 12.9 mm X 0.5mm~6mm		**GM NH3**	250	cm^3*min-1
R	8.314	Jmol^-1K^-1			

The experimental case thickness or nitrided layer thickness of the nitrided austenitic stainless steel at 600°C are measured and recorded as per table 4.5.2 below.

Table 4.5.2 Nitrided layer thickness for gas nitriding of 316L at nitriding temperature of 600°C

Nitrided layer thickness for 316L at 600°C	
Nitriding (Hour)	Measured Thickness (mm)
2	0.030
8	0.052
24	0.112
48	0.128

The diffusion coefficients based on the experimental parameters are calculated to be as per table 4.5.3.

Table 4.5.3 Diffusion Coefficients for Gas Nitriding of 316L at 600°C

Diffusion Coefficients	
Dα	1.43995E-11
Dγ'	2.51749E-13
Dε	5.32805E-14

The calculated estimated growth of ε – phase structure of the gas nitrided 316L SS at 600°C are as per table 4.5.4.

Table 4.5.4 Calculated thickness of ε – phase layer for gas nitrided 316L SS at 600ºC

Calculated thickness for ε-phase layer structure	
Nitriding Hour (H)	**Calculated Thickness (mm)**
2	3.42339E-05
8	6.84678E-05
24	0.000135697
48	0.000191905

The calculated estimated growth of γ' – phase structure of the gas nitrided 316L SS at 600ºC are as per table 4.5.5 below.

Table 4.5.5 Calculated thickness of γ' – phase layer for gas nitrided 316L SS at 600ºC

Calculated thickness for γ'-phase layer structure	
Nitriding Hour (h)	Calculated Thickness (mm)
2	0.026927976
8	0.053855951
24	0.093281244
48	0.131919601

The total estimated nitrided layer thickness for gas nitrided 316L SS at 600ºC are as per table 4.5.6 which also composed of the actual measured thickness of the nitrided layer by Patthi as a comparison to the calculated thickness values.

Table 4.5.6 Total Calculated thickness versus measured thickness for gas nitrided 316L at 600ºC

Layer Nitrided Below Surface 600ºC (mm)			
Nitriding Hour	Measured Thickness	Calculated Thickness (γ'+ε)	|Δ Thickness|
2	0.030	0.027	0.003
8	0.052	0.054	0.002
24	0.112	0.093	0.019
48	0.128	0.132	0.004

Conclusion

The graphical representation of the calculated values (estimated thickness) and the actual experimental values is shown in figure 4.1 which clearly indicates the

similarities and differences between the actual experimental values and the calculated or estimated thickness values. The calculated values and the actual experimental values are in close agreement with each other and thus indicate that the equation manage to predict the nitrided layer thickness. This is proven by the fact that the equation manage to predict the thickness of the nitrided layer up to the range of ± 5μm for three out of four readings. In conclusion, the mathematical model manage to successfully predict the nitrided layer thickness for austenitic stainless steel (AISI 316L) at temperature of 600^{o}C for a nitriding duration between 2 hours up to 48 hours.

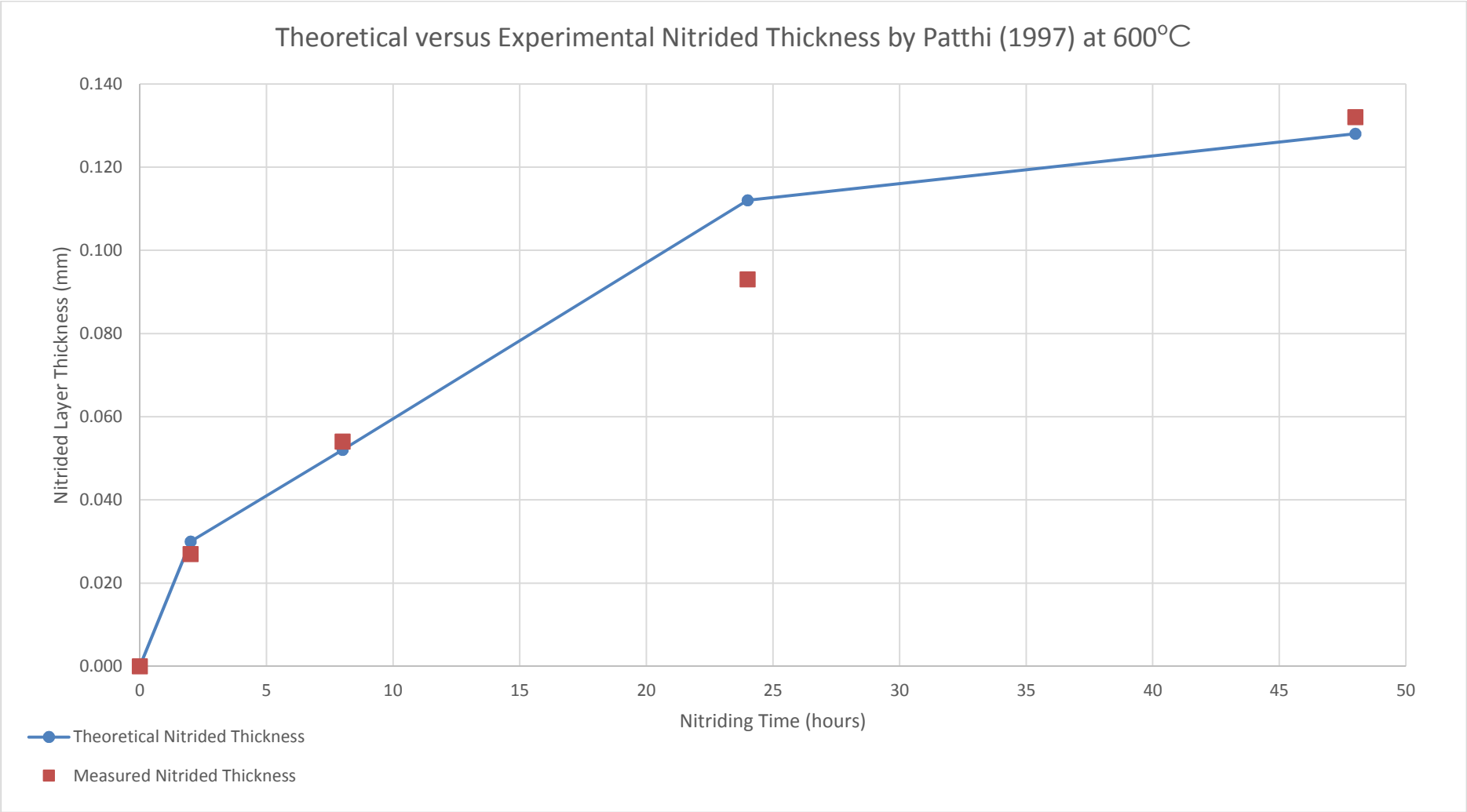

Figure 4.1 Nitrided layer thickness (mm) vs. nitriding hour for 600°C

4.6 Gas Nitriding: Calculation result for 700°C in comparison to Patthi (1997) for AISI 316L SS [24]

Below are the experimental parameter details from the reference [24] which is indicated in table 4.6.1. The experiment were carried out to investigate the thickness of the nitrided layer after 22, 28 and 48 hours of gas nitriding. The material used for the experiment are AISI 316L SS plates. The experiment is a single stage gas nitriding process where the nitriding process is done at a single nitriding temperature, in this case 700°C.

Table 4.6.1 Experimental details for Patthi 316L nitriding at 700°C

Experimental Details					
Time	[0 22 28 48] Hour(s)		**Nitrogen Flow rate**	200	cm^3*min-1
Temperature	973	Kelvin	**GM H2**	100	cm^3*min-1
Sample Size	12.9 mm X 12.9 mm X 0.5mm~6mm		**GM NH3**	250	cm^3*min-1
R	8.314	Jmol^-1K^-1			

Table 4.6.2 Nitrided layer thickness for gas nitriding of 316L at nitriding temperature of 700°C

Nitrided layer thickness for 316L at 700°C	
Nitriding (Hour)	Measured Thickness (mm)
8	0.092
22	0.136
28	0.140
48	0.152

The diffusion coefficients based on the experimental parameters are calculated to be as per table 4.6.3 below.

Table 4.6.3 Diffusion Coefficients for Gas Nitriding of 316L at 700°C

Diffusion Coefficients	
Dα	4.33911E-11
Dγ'	6.23077E-13
Dε	2.00291E-13

The calculated estimated growth of ε – phase structure of the gas nitrided 316L SS are as per table 4.6.4.

Table 4.6.4 Calculated thickness of ε – phase layer for gas nitrided 316L SS at 700^{o}C

Calculated thickness for ε-phase layer structure	
Nitriding Hour (H)	**Calculated Thickness (mm)**
8	0.000139587
22	0.000231479
28	0.000284178
48	0.000372077

The calculated estimated growth of γ’ – phase structure of the gas nitrided 316L SS are as per table 4.6.5.

Table 4.6.5 Calculated thickness of γ’ – phase layer for gas nitrided 316L SS at 700^{o}C

Calculated thickness for γ’-phase layer structure	
Nitriding Hour (H)	**Calculated Thickness (mm)**
0	0
8	0.076874786
22	0.12748241
28	0.143819555
48	0.188303999

The total calculated nitrided layer thickness for gas nitrided AISI 316L SS at 700^{o}C by Patthi are as per table 4.6.6 which also composed of the actual measured thickness of the nitrided layer as a comparison to the calculated thickness.

Table 4.6.6 Total Calculated thickness versus measured thickness for gas nitrided AISI 316L SS at 700^{o}C

Layer Nitrided Below Surface 700^{o}C			
Nitriding Hour	Measured Thickness	Calculated Thickness (γ'+ε)	|Δ Thickness|
8	0.092	0.077	0.015
22	0.136	0.128	0.008
28	0.140	0.144	0.004
48	0.152	0.189	0.037

Conclusion

The graphical representation of the calculated values (estimated thickness) and the actual experimental values is shown in figure 4.2 which clearly indicates the similarities and differences between the actual experimental values and the calculated or estimated thickness values. The calculated values and the actual experimental values are in close agreement with each other and thus indicate that the equation manage to predict the nitrided layer thickness. The mathematical model manage to predict up to ±10 µm for two out of four readings while the other two readings vary at a quite large values that is 15µm and 37 µm, however, this values are considerably small (16 to 24% percentage error). In conclusion, the mathematical model manage to successfully predict the nitrided layer thickness for austenitic stainless steel (AISI 316L) at temperature of 700^{o}C for a nitriding duration between 8 hours up to 48 hours.

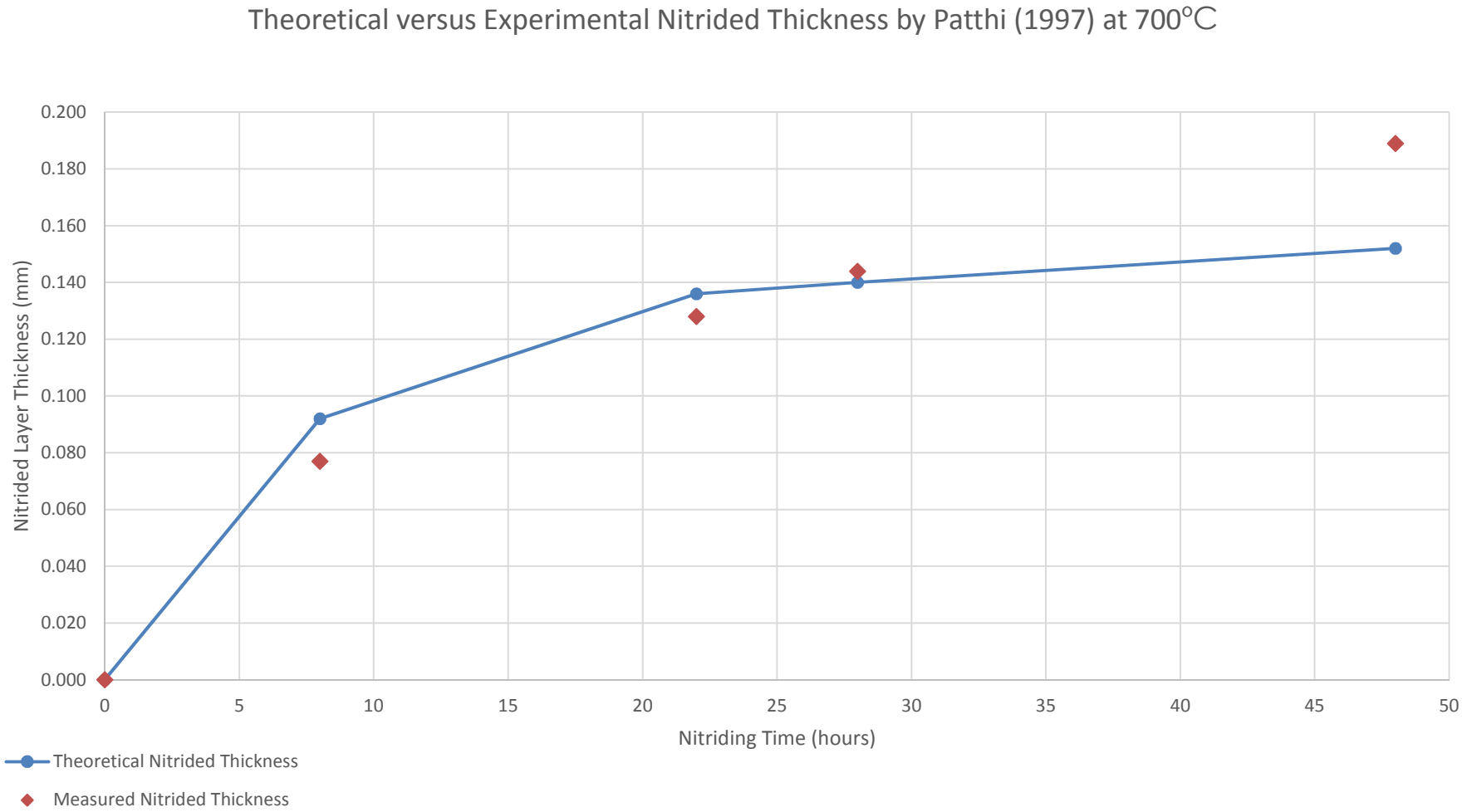

Figure 4.2 Nitrided layer thickness (mm) vs. nitriding hour for 700°C

4.7 Gas Nitriding: Calculation result for 550ºC in comparison to K. Subramaniam and N.T. Ansari for gas nitriding of AISI 316LSS [25]

The result from the experiment from the reference [25] are for the 12 hours at for 550ºC. The reading are as per 52.6μm (normal nitriding process as per the nitriding process used as per reference [24] but maintained at the highest temperature, 550^0C for 8 hours in single state), 68.9 μm ((normal nitriding process as per the nitriding process used as per reference [24] but maintained at the highest temperature, 550^0C for 11 hours in single state), and 60.3 μm (the nitriding process is double stage for 500ºC for 5 hours and 550ºC for 4 hours) which are based on three different nitriding method in which the author will not be discussing in length (but are explained in the bracket). The calculation for the estimated thickness are as per calculation below. The diffusion coefficients are as per table 4.7.1 below.

Table 4.7.1 Diffusion Coefficients for Gas Nitriding of 316L at 550ºC

Diffusion Coefficients	
Dα	7.50176E-12
Dγ'	1.47337E-13
Dε	2.43564E-14

The calculated estimated growth of ε – phase structure of the gas nitrided 316L SS are as per table 4.7.2

Table 4.7.2 Calculated thickness of ε – phase layer for gas nitrided 316L SS at 550ºC

Calculated thickness for ε-phase layer structure	
Nitriding Hour (H)	**Calculated Thickness (mm)**
12	6.48752E-05

The calculated estimated growth of γ' – phase structure of the gas nitrided 316L SS at 550ºC are as per table 4.7.2

Table 4.7.3 Calculated thickness of γ’ – phase layer for gas nitrided 316L SS at 550^{o}C

Calculated thickness for γ’-phase layer structure	
Nitriding Hour (H)	**Calculated Thickness (mm)**
12	0.053027873

The total estimated nitrided layer thickness for gas nitrided 316L SS at 550^{o}C by Subramaniam et al. are as per table 4.7.3which also composed of the actual measured thickness of the nitrided layer as a comparison to the calculated thickness.

Table 4.7.4 Total Calculated thickness for gas nitrided 316L at 550^{o}C

Total nitrided Layer thickness (mm)	
Nitriding Hour	**Estimated Thickness (γ'+ε)**
12	0.053092748

The total calculated nitrided layer thickness for gas nitrided AISI 316L SS at 550^{o}C by K. Subramaniam and N.T. Ansari are as per table 4.7.5 which also composed of the actual measured thickness of the nitrided layer as a comparison to the calculated thickness.

Table 4.7.5 Total Calculated thickness versus measured thickness for gas nitrided AISI 316L SS at 550^{o}C for experiment by K. Subramaniam and N.T. Ansari

Layer Nitrided Below Surface 550^{o}C for 12 hours (mm)			
Nitriding Technique	Measured Thickness	Calculated Thickness (γ'+ε)	|Δ Thickness|
Single stage (maintained at 550^{o}C for 8 hours)	0.0526	0.053	0.0004
Single Stage (maintained at 550^{o}C for 11 hours)	0.0689	0.053	0.0159
Double stage (500^{o}C for 5 hours and 550^{o}C for 4 hours)	0.0603	0.053	0.0073

Conclusion

As mention earlier, the experimental result from the result varies a 52.6 μm, 68.9 μm and 60.3 μm and based on the calculation result, the estimated or calculated nitrided layer thickness is at the value of 0.053 mm which is really close to the first value (52.6 μm) and the third value (60.3 μm) are really close to the calculated value but the second value (68.9 μm) is quite far away. This is due to the difference in technique that the author of the particular paper used in the gas nitriding process. The typical nitriding technique that is the second technique that is the one that produces the largest difference in thickness between the experimental and the calculated value. However, the mathematical model still manage to give a rough estimate of the actual nitrided layer thickness by 0.016mm which is quite good given the complexity of the diffusion mechanism.

For graphical and conceptual purposes, the author extended the calculation to predict up to the same period of study as was done by Patthi (1997) that is to the total nitriding time of 48 hours and the table bellows shows the calculated theoretical nitrided thickness layer.

Table 4.7.6 the theoretical nitrided layer thickness at 550°C gas nitriding

Hour (s)	Calculated Thickness (mm)
0	0.000
8	0.043
12	0.053
28	0.081
48	0.106

Figure 4.3 shows the graphical representation of the theoretical nitrided layer thickness versus up to 48 hours of nitriding time. The actual nitrided layer thickness is also presented in the form of points so that the difference between the experimental values and the theoretical values is clearly seen.

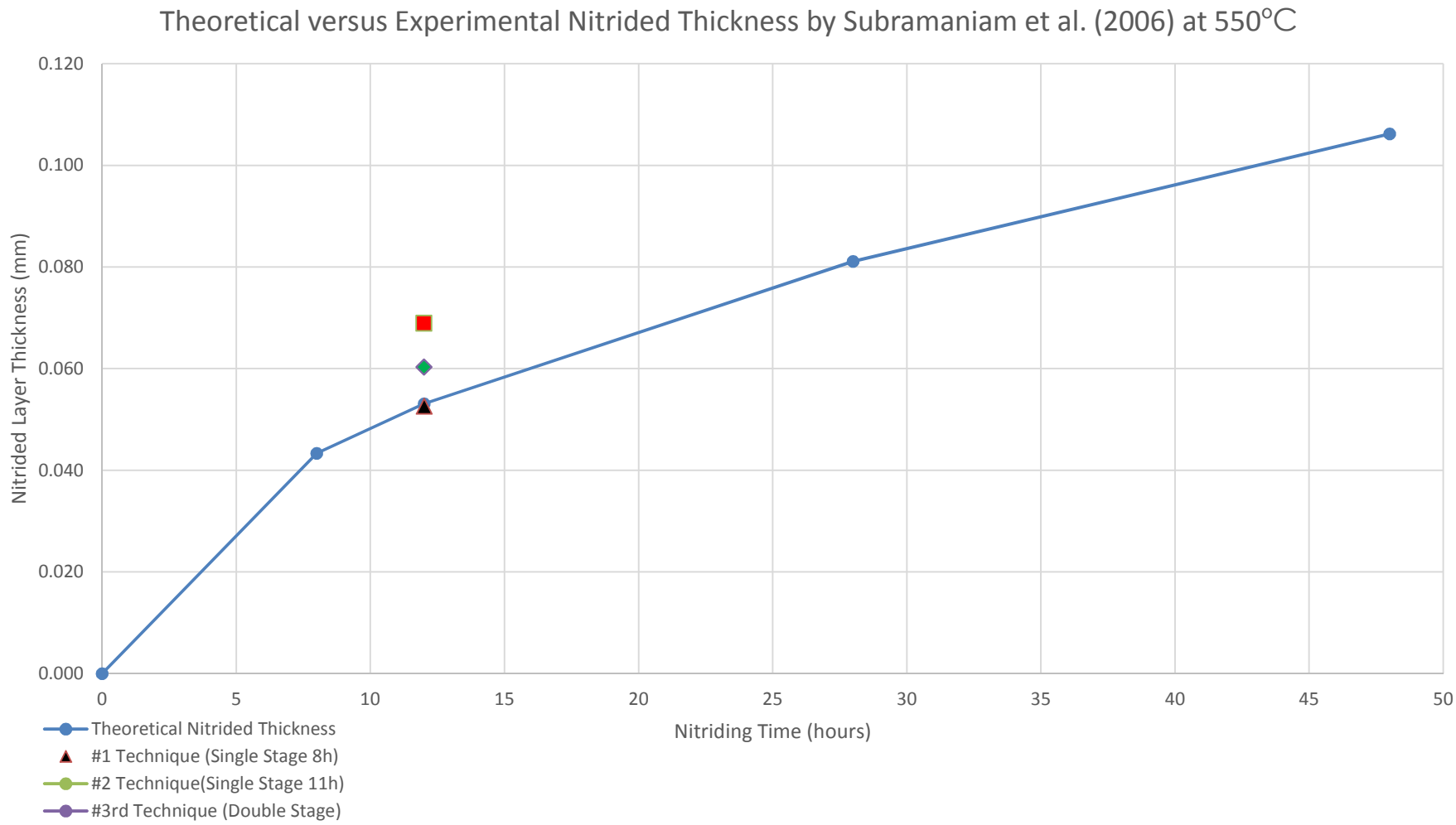

Figure 4.3 Nitrided layer thickness versus nitriding time for gas nitriding at 550°C

4.8 Discussion and conclusion on the validity of the equation with respect to the gas nitrided austenitic stainless steel.

Based on the comparison between the calculated thickness of the nitrided layer and that of the experimental or actual measured values of the nitrided thickness by Patthi [24] and Subramaniam et al. [25]. The actual and the calculated values are in close agreement which shows that the mathematical model represent the nitrided layer growth of gas nitrided of AISI 316L stainless steel almost accurately. Therefore, this have proven that, the mathematical model manage to predict the nitrided layer thickness of AISI 316L SS with varying nitriding time and temperature up to very good accuracy as seen in comparison with the experimental result from Patthi [24] and K. Subramaniam and N.T. Ansari [25].

The summary of the theoretical versus the experimental nitrided thickness for gas nitrided AISI 316L SS is shown in figure 4.5, in the next page, indicating that there are a good agreement between the theoretical nitrided thickness versus the actual experimental nitrided thickness. However, there are some difference in the actual versus the theoretical value. Therefore, it is important to be reminded and re-instated that, the mathematical model is only accounted for one out of three key parameter in determining the nitrided layer thickness (as seen in literature review section 2.2). Therefore the other two unaccounted factors, namely, the nitrogen dissociation and the nitriding potential. These two factors are harder to control in gas nitriding as compared to plasma nitriding in which the chemistry as that of gas nitriding.

In conclusion, based on the Figure 4.5 we can conclude that the mathematical model manage to predict the nitrided layer thickness of the low temperature gas nitriding with respect only to one key parameter in the gas nitriding process control, that is the nitriding temperature with very good accuracy. This is supported from the fact that the difference between the experimental and theoretical (calculated) nitrided layer thickness is calculated to be maximum at 0.037 mm (Patthi (1997) for 700^{o}C) which is still in good agreement (0.152mm for measured thickness and 0.189mm for calculated thickness).

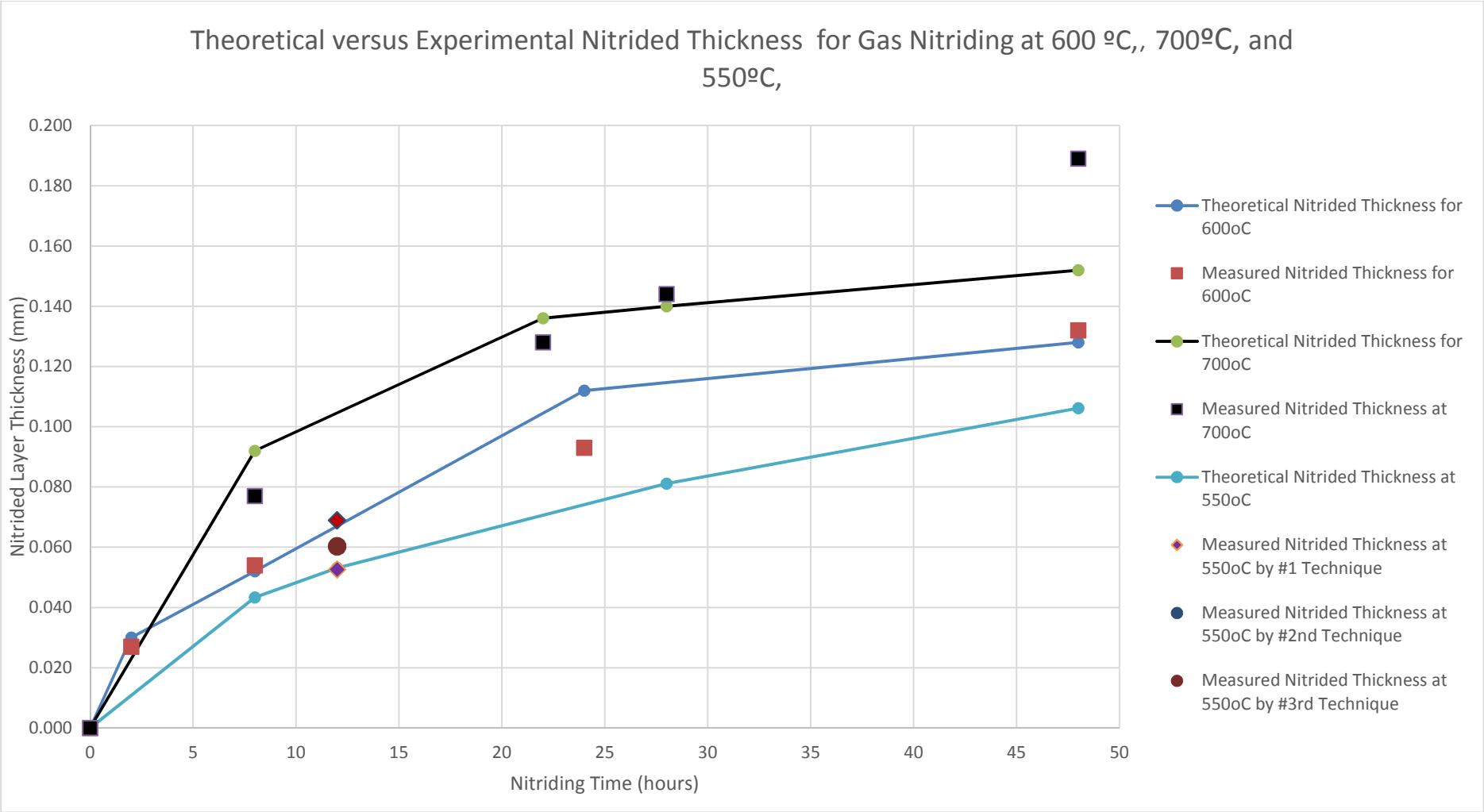

Figure 4.4 Theoretical versus experimental nitrided thickness for gas nitriding at 600°C, 700 °C and 550 °C

4.9 Plasma Nitriding: Calculation result for 407ºC in comparison to plasma nitrided AISI 316L SS by N. Renevier, P. Collignon, H. Michel, and T. Czerwiec (1999) [26]

The plasma nitriding device shown in Figure 4.4 derives from the thermionic arc evaporation process patented and used by Balzers for ion plating physical vapour deposition (PVD). A high current (100-300 A), low voltage (25-40 V) thermionic arc is generated in argon in an ionisation chamber (1 on Fig. 4.4) mounted on the top of the nitriding reactor itself. Segmented anodes (2 and 3 on Fig. 4.4) distributed in the reactor spread the discharge in the whole processing chamber to create a uniform low-pressure plasma (0.4-0.8 Pa). A heated substrate holder (4 on Figure 4.5) is used to provide a uniform temperature on the substrates.

Prior to the nitriding process, these substrates were mechanically polished (final stage 1µm) and ultrasonically cleaned in alcohol. An optimised nitriding procedure in two stages has previously been determined. The first stage is an in situ cleaning treatment performed to remove the surface oxide layers. Such a cleaning treatment must be adapted to the material to be treated. As chemical etching in Ar-H_2 gas mixture is performed at floating potential (see table 4.9.1 for processing conditions) gives low surface roughness, it is used for AISI 316L stainless steel substrate cleaning.

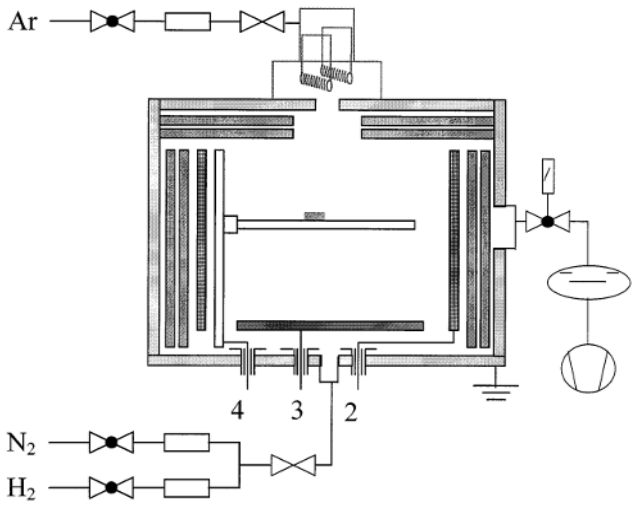

Figure 4.5. Schematic diagram of the main components of the low pressure arc discharge for nitriding. (1) Plasma beam holder; (2) cylindrical anode; (3) flat anode; and (4) heating substrate holder.

Table 4.9.1 Experimental conditions

Processing Parameter	Cleaning	Nitriding
Time (h)	1.5	0.08-9
Total pressure (Pa)	0.5	0.8
Bias voltage (V)	Floating	Floating
Temperature (ºC)	407	407
Argon pressure (Pa)	0.4	0.4
Hydrogen	Yes	No
Nitrogen pressure (Pa)	0	0.4
Arc intensity (A)	120 on each anode	-
Arc tension (V)	20-30	30-34

The diffusion coefficients for plasma nitriding of AISI 316L SS at 407ºC is shown in the table 4.9.2.

Table 4.9.2 Diffusion Coefficients for plasma nitriding of AISI 316L SS at 407ºC

Diffusion Coefficients	
Dα	6.84524E-13
Dγ'	2.06096E-14
Dε	1.37528E-15

The calculated estimated growth of ε – phase structure of the plasma nitrided AISI 316L SS at 407ºC are as per table 4.9.3

Table 4.9.3 Calculated thickness of ε – phase layer for plasma nitrided AISI 316L SS at 407ºC

Calculated thickness for ε-phase layer structure	
Nitriding Hour (h)	**Calculated Thickness (mm)**
1	2.22825E-06
2	3.15122E-06
5	9.95089E-06
7.5	1.21873E-05

The calculated estimated growth of γ' – phase structure of the plasma nitrided AISI 316L SS at 407ºC are as per table 4.9.4.

Table 4.9.4 Calculated thickness of γ’ – phase layer for plasma nitrided AISI 316L SS at 407ºC

Calculated thickness for γ’-phase layer structure	
Nitriding Hour (H)	**Calculated Thickness (mm)**
1	0.076874786
2	0.12748241
5	0.143819555
7.5	0.188303999

The total estimated nitrided layer thickness for plasma nitrided AISI 316L SS at 407ºC by Revenier et al. are as per table 4.9.5 which also composed of the actual measured thickness of the nitrided layer as a comparison to the calculated thickness.

Table 4.9.5 Total Calculated thickness, calculated thickness and difference between the experimental thickness and calculated thickness for plasma nitrided AISI 316L SS at 407ºC

Layer Nitrided AISI 316L SS at 407ºC (mm)			
Nitriding Hour	measured thickness	Calculated Thickness (γ'+ε)	|Δ Thickness|
1	0.004240	0.005781947	0.0015
2	0.005477	0.008176908	0.0027
5	0.008062	0.012933796	0.0049
7.5	0.010000	0.0158406	0.0058

Conclusion

This is a comparison between the predicted nitrided thicknesses from the mathematical model for the plasma nitriding experiment of AISI 316L SS at 407ºC between nitriding duration of 1 up to 7.5 hours. As shown in table 4.9.5 above the mathematical model manage to predict all the points very accurately. This is proven by the fact that the largest different between the actual and experimental values is at 0.0058 mm which is relatively very small in comparison to the comparison done with respect to gas nitriding of AISI 316L SS as seen previously in section 4.5, 4.6, and 4.7 where the difference in the actual and predicted thickness is relatively larger.

This is possibly the result of inefficiency in the gas nitriding process as a comparison to that of plasma nitriding (arc glow discharge) process.

The graphical representation of the theoretical and experimental nitrided thickness value for plasma nitrided AISI 316L SS at 407^{o}C is shown in Figure 4.6.

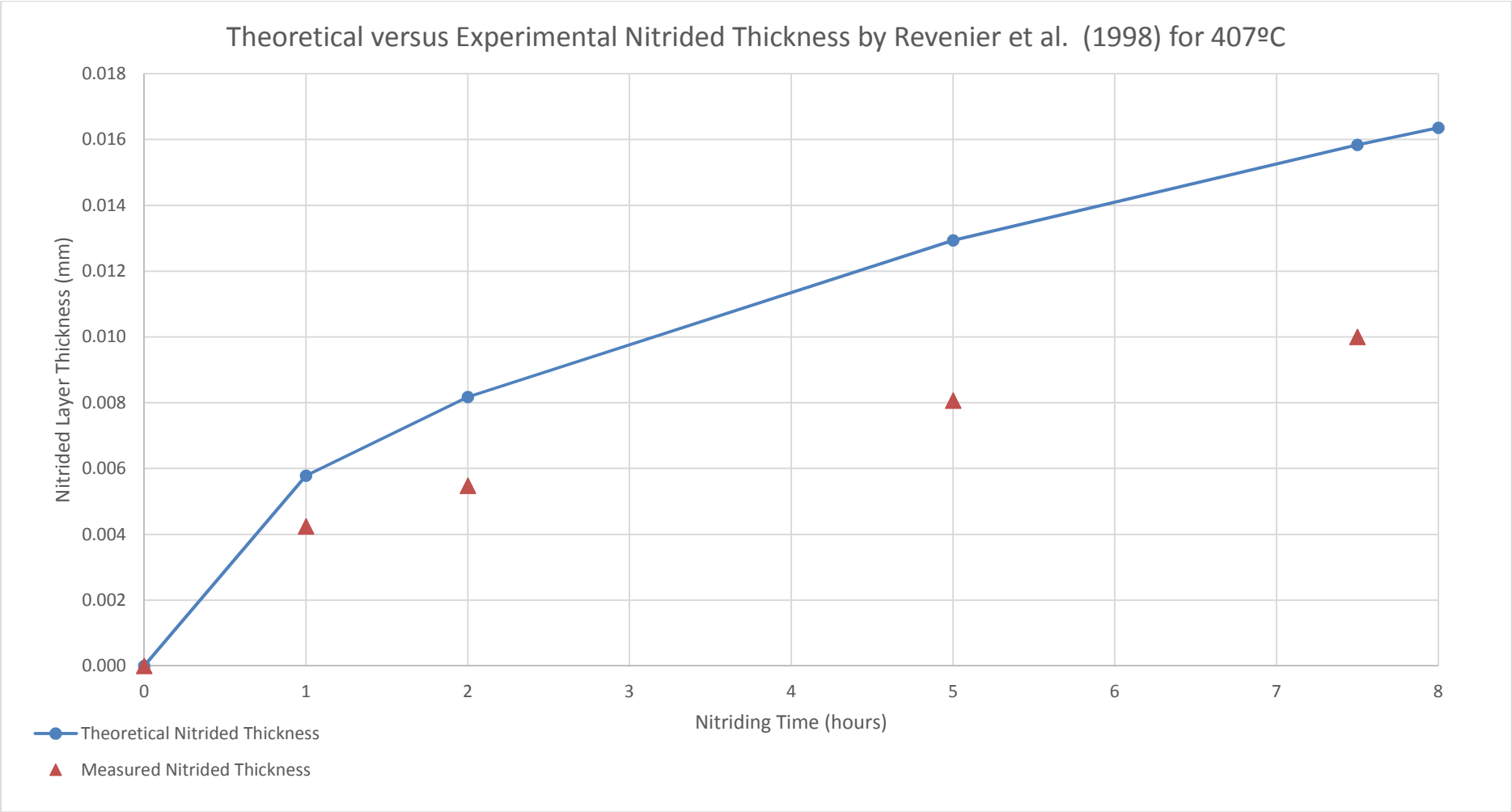

Figure 4.6 Theoretical versus experimental nitrided layer thickness by Revenier et al. (1998) for plasma nitriding at 407°C

4.10 Plasma Nitriding: Calculation result for 430ºC in comparison to plasma nitrided (glow discharge) AISI 316L SS by A. Fossati, F. Borgioli, E. Galvanetto and T. Bacci (2006) [27]

Experimental procedure

Prismatic samples (40x18x4 mm) were obtained from an AISI 316L steel annealed bar (diameter 60 mm) by cutting, grinding and polishing up to 6 μm diamond suspension.

Before the plasma nitriding process, the samples were ultrasonically cleaned in an acetone bath for 10 minutes. Glow-discharge treatments were performed in a laboratory plasma equipment, similar to industrial ones, using a DC power supply. The furnace system had an axial symmetry. Samples were fastened by means of screws at each face of the prismatic sample holder. The samples and the sample holder, placed in the centre of the treatment chamber, worked as cathode and were completely surrounded by a cylindrical metal screen made up of AISI 304 SS which was grounded and worked as anode. The anode-cathode distance was about 60 mm. Gas composition (80% N_2 and 20% H_2) was fixed during the sputtering step and the nitriding treatments. The treatment temperature was measured by a thermocouple inserted in the sample holder and controlled by varying the discharge current from the DC current supply. Nitriding treatments were performed at 703K (430ºC) at a working pressure of 10^3 Pa for times in the range of 0-5h. The current density necessary to maintain constant the temperature during the nitriding treatment was 2.6 ± 0.1 mA cm^{-2}, while the measure voltage drop between the electrodes was 175±5V. Before the nitriding treatments samples were warmed up to 653 K by means of a cathodic sputtering in order to remove the natural passive film and enables a homogeneous and correct nitriding process. after the sputtering step, the pressure and the temperature were increased up to their nominal values; the 0-h treatment consisted in the cathodic sputtering up to 653K (380ºC) and just in the raising in temperature up to 703K (430 ºC), then the power supply was turned off and the chamber evacuated.

The diffusion coefficients of the plasma nitriding process are as follow per table 4.10.1.

Table 4.10.1 Diffusion Coefficients for plasma nitriding of AISI 316L SS at 430^{o}C

Diffusion Coefficients	
Dα	1.07442E-12
Dγ'	2.98482E-14
Dε	2.36278E-15

The calculated estimated growth of ε – phase structure of the plasma nitrided AISI 316L SS at 430^{o}C are as per table 4.10.2

Table 4.10.2 Calculated thickness of ε – phase layer for plasma nitrided AISI 316L SS at 430^{o}C

Calculated thickness for ε-phase layer structure	
Nitriding Hour (H)	**Calculated Thickness (mm)**
1	3.54025E-06
2	5.00666E-06
3.5	1.09126E-05
5	1.3043E-05

The calculated estimated growth of γ' – phase structure of the plasma nitrided AISI 316L SS at 430^{o}C are as per table 4.10.3.

Table 4.10.3 Calculated thickness of γ' – phase layer for plasma nitrided AISI 316L SS at 430^{o}C

Calculated thickness for γ'-phase layer structure	
Nitriding Hour (H)	**Calculated Thickness (mm)**
1	0.007284837
2	0.010302315
3.5	0.013628681
5	0.01628939

The total estimated nitrided layer thickness for plasma nitrided AISI 316L SS at 430^{o}C by Revenier et al. are as per table 4.10.4 which also composed of the actual measured thickness of the nitrided layer as a comparison to the calculated thickness.

Table 4.10.4 Total Calculated thickness, calculated thickness and difference between the experimental thickness and calculated thickness for plasma nitrided AISI 316L SS at 430^{o}C

Layer Nitrided Below Surface			
Nitriding Hour	measured thickness	Calculated Thickness ($\gamma'+\varepsilon$)	$\lvert\Delta$ Thickness$\rvert$
1	0.007000	0.007288377	0.000288
2	0.008000	0.010307321	0.002307
3.5	0.010000	0.013639594	0.003640
5	0.013000	0.016302433	0.003302

Conclusion

This is the plasma nitrided layer of AISI 316L SS at 430^{o}C by Fossati et al. shows a very positive feedback to the validity of the mathematical model which is in similar fashion to the result for the for plasma nitriding of similar material conducted by Revenier et al. The difference between the measured thickness and calculated thickness is relatively very small and the largest recorded at 0.0036 mm. Hence, this shows that the mathematical model is highly accurate in predicting the nitrided layer thickness of the plasma nitrided AISI 316L SS which is the same conclusion from derived based on the plasma nitriding process by Revenier et al.

The graphical representation of the calculated thickness versus the experimental ones are as per figure 4.7.

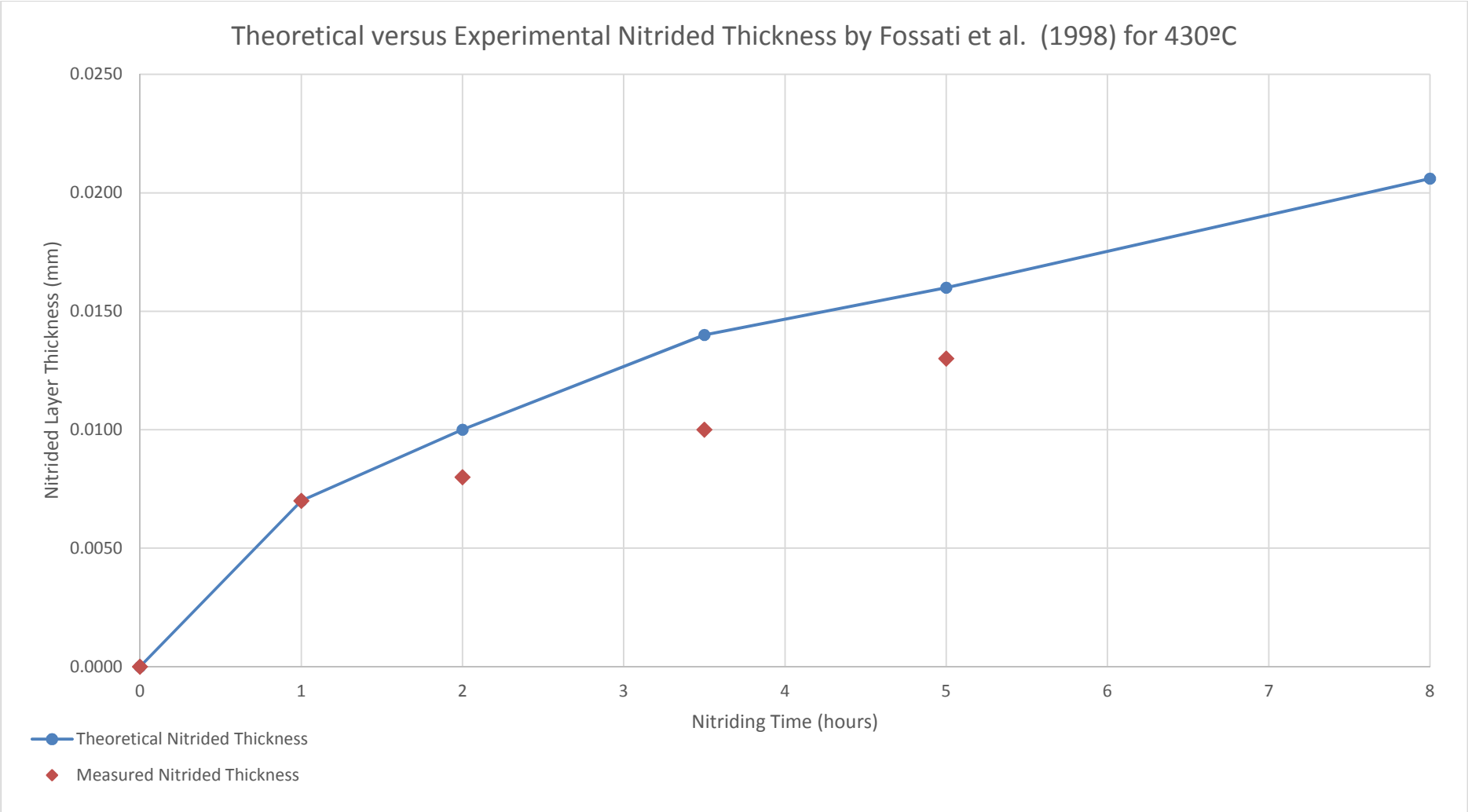

Figure 4.7 Theoretical versus experimental nitrided layer thickness by Fossati et al. (2006) for plasma nitriding at 430°C

4.11 Plasma Nitriding: Calculation result for 450ºC in comparison to plasma nitrided of AISI 316L SS M. Tsujikawa et al. (2005) [28]

Experimental procedure

The substrate material used in this work is AISI 316L stainless steel. The solution-treated steel bars were cut into 25mm x 50 mm x 5 mm. The faces of the plates were then ground and polished to the mirror finish.

Plasma thermochemical treatment was performed with a laboratory type apparatus with a DC power source. Each specimen attached with a thermocouple was set in the furnace as a cathode. After evacuation up to $1.33 \cdot 10^{-1}$ Pa, the mixed gas pressure for each specimen was adjusted to $6.67 \cdot 10^{2}$ Pa. All plasma thermochemical treatment in this study was carried out at 723 K (450ºC). Total respective processing times were 8 h. The specimen was plasma nitriding treated at 723 K (450ºC) with a mixture of 80% nitrogen gas and 20% hydrogen gas for 8 h.

The diffusion coefficient for the said experimental parameter are as per table 4.11.1 below.

Table 4.11.1 1 Diffusion Coefficients for plasma nitriding of AISI 316L SS at 450ºC

Diffusion Coefficients	
Dα	1.55343E-12
Dγ'	4.04081E-14
Dε	3.67828E-15

The calculated estimated growth of ε – phase structure of the plasma nitrided AISI 316L SS at 450ºC are as per table 4.11.2

Table 4.11.2 Calculated thickness of ε – phase layer for plasma nitrided AISI 316L SS at 450ºC

Calculated thickness for ε-phase layer structure	
Nitriding Hour (H)	**Calculated Thickness (mm)**
8	1.38198E-05

The calculated estimated growth of γ' – phase structure of the plasma nitrided AISI 316L SS at 450ºC are as per table 4.11.3.

Table 4.11.3 Calculated thickness of γ' – phase layer for plasma nitrided AISI 316L SS at 450°C

Calculated thickness for γ'-phase layer structure	
Nitriding Hour (H)	**Calculated Thickness (mm)**
8	0.024205129

The total estimated nitrided layer thickness for plasma nitrided AISI 316L SS at 450°C by Tsujikawa et al. are as per table 4.11.4 which also composed of the actual measured thickness of the nitrided layer as a comparison to the calculated thickness of the nitrided layer.

Table 4.11.4 Total Calculated thickness, calculated thickness and difference between the experimental thickness and calculated thickness for plasma nitrided AISI 316L SS at 450°C

Experimental Vs Estimated Result (mm)		
Temp(°C)	**Hour (H)**	8
450	Experimental	0.0165
	Calculated	0.0242
	|Δ Thickness|	0.007718949

Conclusion

As seen in table 4.11.4, the difference in the thickness between the experimental and calculated thickness is valued at 0.0077 mm which is very small when compared to that of the gas nitriding treated. This result also act as a compliment to the result by N. Revenier et al. and A. Fossati et al. All these plasma nitrided AISI 316L shows positive indication that the mathematical model manage to predict the nitrided layer thickness up to a very good accuracy. For analysis and conceptual purpose, the author have calculated the theoretical nitrided layer thickness for plasma nitriding of AISI 316L at 450°C from 0 to 8 hours and the values are as per recorded on table 4.11.5 below.

Table 4.11.5 the theoretical nitrided layer thickness of plasma nitrided AISI 316L at 450 ℃

Hour (s)	Theoretical Thickness (mm)
0	0.0000
1	0.0086
2	0.0121
5	0.0192
8	0.0242

The graphical representation of the nitrided layer thickness for plasma nitriding at 450℃ is shown in figure 4.8.

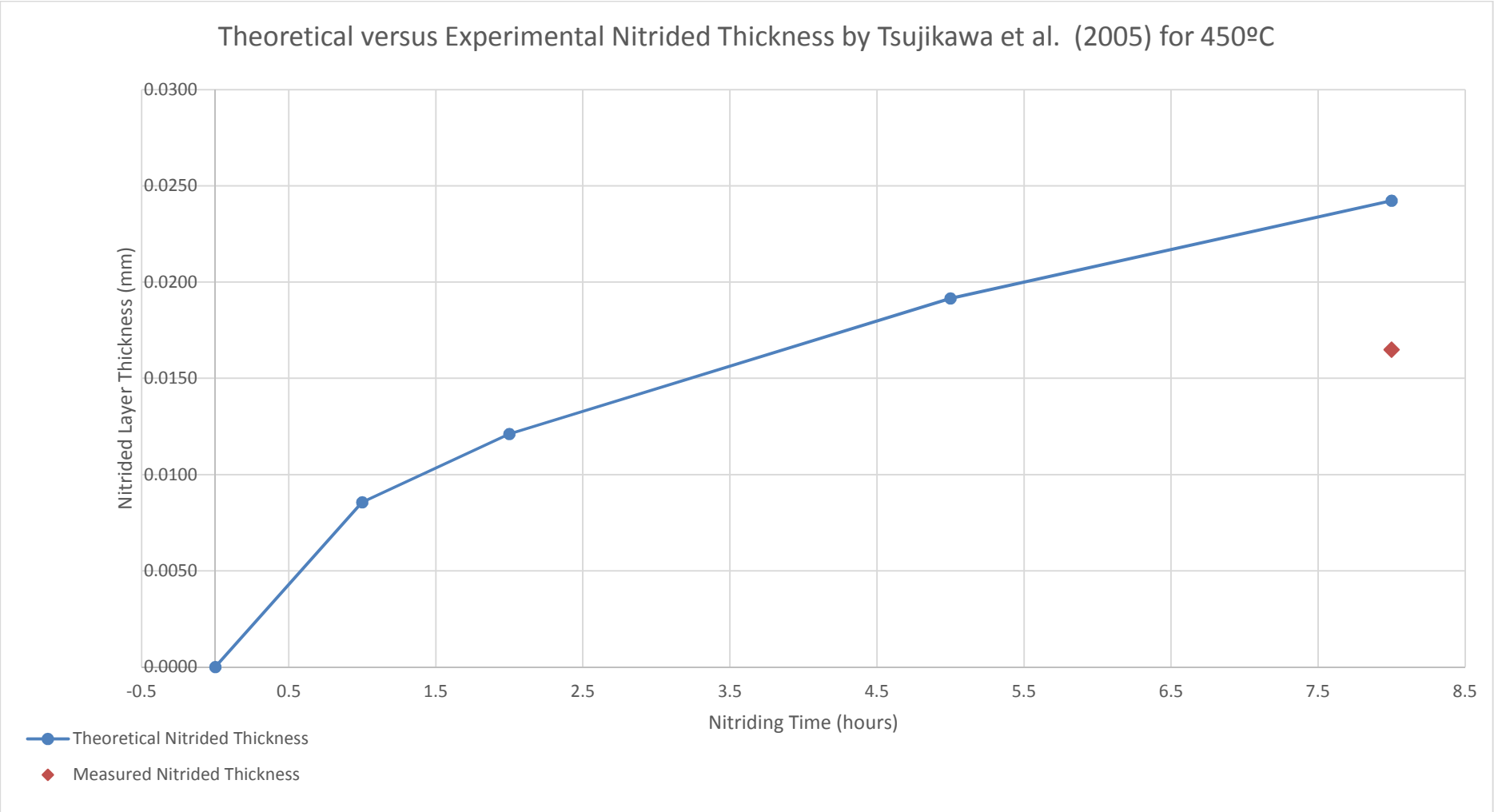

Figure 4.8 Theoretical versus experimental nitrided layer thickness by Tsujikawa et al. (2005) for plasma nitriding at 450°C

4.12 Discussion and conclusion on the validity of the equation with respect to the plasma nitrided austenitic stainless steel.

Based on the comparison between the calculated thickness of the nitrided layer and that of the experimental or actual measured values of the nitrided thickness by Revenier et al. [26] Fossati et al. [27] and Tsujikawa et al. [28]. The actual and the calculated values are in close agreement which shows that the mathematical model represent the nitrided layer growth of plasma nitrided of AISI 316L stainless steel accurately. Therefore, this have proven that, the mathematical model manage to predict the nitrided layer thickness of AISI 316L SS with varying nitriding time and temperature up to very good accuracy as seen in the graphical form in figure 4.9.

Figure 4.9 (in the next page) is the graphical summary of the theoretical and actual experimental nitrided thickness values for plasma nitriding at 407°C, 430 °C and 450°C. However, there are some difference in the actual versus the theoretical value. Therefore, it is important to be reminded and re-instated that, the mathematical model is only accounted for one out of three key parameter in determining the nitrided layer thickness (as seen in literature review section 2.2). Therefore the other two unaccounted factors, namely, the nitrogen dissociation and the nitriding potential. These two factors are harder to control in gas nitriding as compared to plasma nitriding in which the chemistry as that of gas nitriding. Hence, the difference between the theoretical and experimental values for plasma nitrided AISI 316L SS is remarkably smaller in comparison to its counterpart in gas nitriding.

In conclusion, based on the Figure 4.9 we can conclude that the mathematical model manage to predict the nitrided layer thickness of the low temperature plasma nitriding with respect only to one key parameter in the plasma nitriding process control, that is the nitriding temperature with very good accuracy. This is supported from the fact that the difference between the experimental and theoretical (calculated) nitrided layer thickness is calculated to be maximum at 0.0077 mm (for Tsujikawa et al.) which is still in good agreement (0.0165mm for measured thickness and 0.0242mm for calculated thickness). In addition, since the control for other two key parameter, nitrogen dissociation and nitriding potential is easier for plasma nitriding, the accuracy of the theoretical nitrided layer thickness increase significantly.

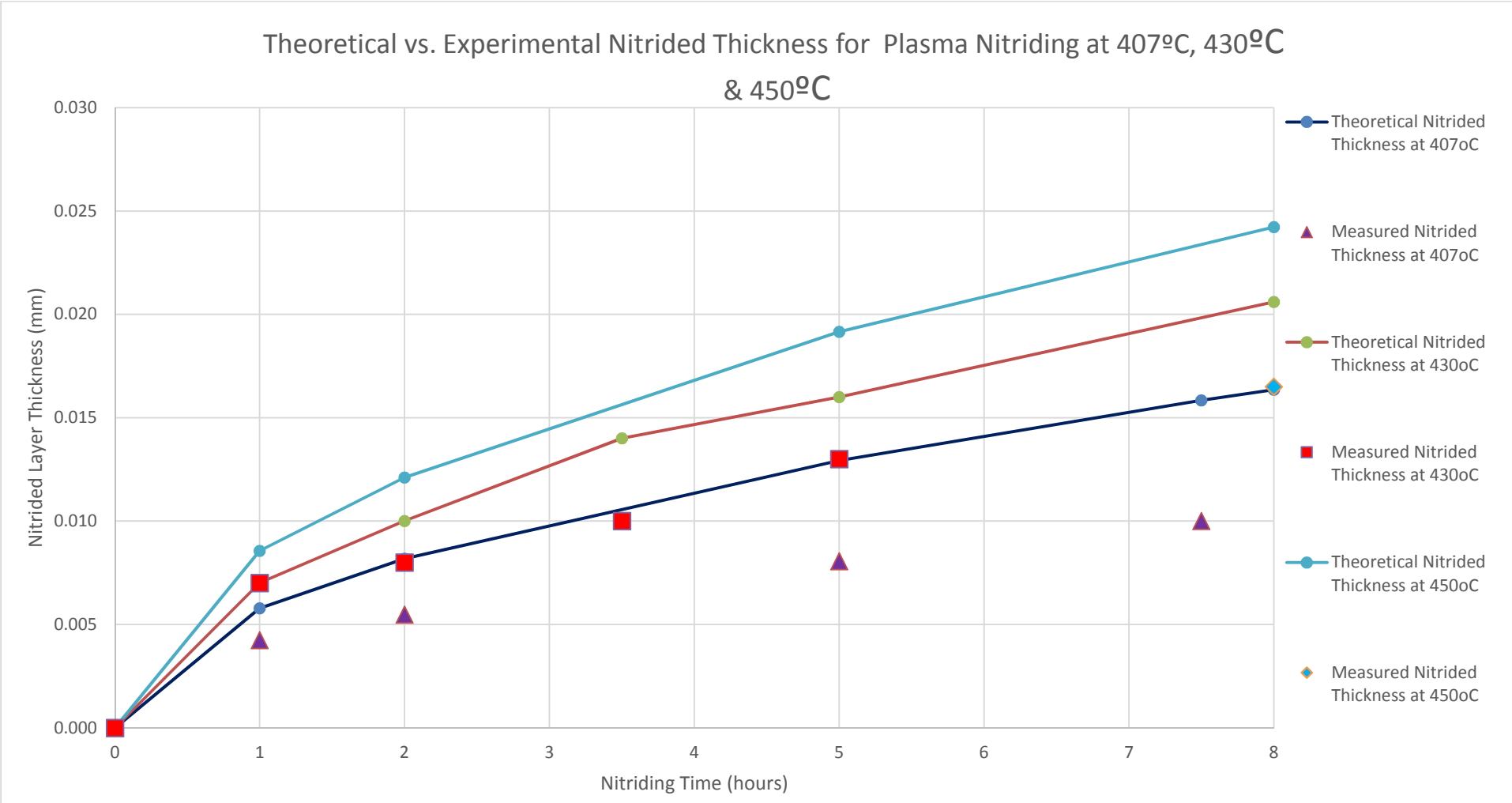

Figure 4.9 Theoretical versus experimental nitrided thickness for plasma nitriding at 407°C, 430 °C and 450 °C

4.13 Summary of Discussion

The mathematical model was develop by Hosseini et al (2007) intended for the application of predicting the nitrided layer thickness for gas nitriding of pure iron and the equations which Hosseini et al developed for pure iron was shown in equation 6 and equation 7. However, the author manage to do a slight alteration for the equation developed by Hosseini et al to fit the equation to the structure formed by gas and plasma nitriding of austenitic stainless steels which can be seen on figure 4.1 and the equations are as per equation 4.17 and equation 4.19.

In order to test the validity of the equation, the author make a comparison between the calculated nitrided thickness layers versus the actual experimental values based on experiments conducted by Patthi (1997) and K. Subramanian and N.T. Ansari (2006) for gas nitriding of AISI 316L SS and experiments conducted by N. Revenier et al. (1999), A. Fossati et al. (2006) and Tsujikawa et al. (2005) for plasma nitriding of AISI 316L SS. The results of the comparison was very promising, especially to the predicting the nitrided layer thickness of plasma nitrided AISI 316L SS. This is due to the fact that the mathematical model managed to predict the nitrided layer thickness of the plasma nitrided AISI 316L up to ±8μm (see Tsujikawa's experimental values section 4.11) which was the largest difference in the calculated thickness versus the experimental thickness recorded for plasma nitrided AISI 316L SS. However, this is not the case for gas nitrided AISI 316L where the largest recorded difference in the calculated thickness versus the experimental thickness was at 0.037 mm (see Patthi's experimental value at section 4.6). However, in general, the mathematical model managed to predict the nitrided layer thickness of AISI 316L SS up to a good accuracy especially in the case of plasma nitrided layer thickness of AISI 316L SS. The summary of the calculated nitrided layer thickness versus the experimental thickness for gas AISI 316L SS are shown in the table 4.13.1 and table 4.13.2 for the its plasma nitrided counterparts.

Table 4.13.1 Summary of the calculated nitrided layer thickness versus the experimental thickness for gas nitrided AISI 316L SS

Layer Nitrided thickness of gas nitrided AISI 316L SS 600°C by Patthi [24] (mm)			
Nitriding Hour	Measured Thickness	Calculated Thickness (γ'+ε)	|Δ Thickness|
2	0.0300	0.0270	0.0030
8	0.0520	0.0540	0.0020
24	0.1120	0.0930	**0.0190**
48	0.1280	0.1320	0.0040
Layer Nitrided thickness of gas nitrided AISI 316L SS at 700°C by Patthi [24] (mm)			
Nitriding Hour	Measured Thickness	Calculated Thickness (γ'+ε)	|Δ Thickness|
8	0.0920	0.0770	**0.0150**
22	0.1360	0.1280	0.0080
28	0.1400	0.1440	0.0040
48	0.1520	0.1890	**0.0370**
Layer Nitrided thickness of gas nitrided AISI 316L SS at 550°C for 12 hours (mm) by Subramaniam et al. [25] (mm)			
Nitriding Technique (for details see section 4.7)	Measured Thickness (12 h)	Calculated Thickness (γ'+ε) (12 h)	|Δ Thickness| (12 h)
Single stage#1	0.0526	0.053	0.0004
Single Stage#2	0.0689	0.053	**0.0159**
Double stage	0.0603	0.053	0.0073

Based on the table 4.13.1 above, the large difference in thickness between the measured and calculated nitrided thickness was calculated to be the largest at 0.037 mm while the others were in the range of 0.015 to 0.019 mm which accounts for 4/11 of the total possible points. Therefore, this shows that the mathematical model manage to predict the nitrided layer thickness for gas nitrided AISI 316L SS fairly.

Table 4.13.2 Summary of the calculated nitrided layer thickness versus the experimental thickness for plasma nitrided AISI 316L SS

Layer nitrided of plasma nitrided AISI 316L SS at 407ºC by N. Revenier [26] (mm)			
Nitriding Hour	Measured thickness	Calculated Thickness (γ'+ε)	|Δ Thickness|
1	0.0042	0.0058	0.0015
2	0.0055	0.0082	0.0027
5	0.0081	0.0129	0.0049
7.5	0.0100	0.0158	0.0058
Layer nitrided of plasma nitrided AISI 316L SS at 430ºC by N. Revenier [27] (mm)			
Nitriding Hour	Measured thickness	Calculated Thickness (γ'+ε)	|Δ Thickness|
1	0.0070	0.0073	0.0003
2	0.0080	0.0103	0.0023
3.5	0.0100	0.0136	0.0036
5	0.0130	0.0163	0.0033
Layer nitrided of plasma nitrided AISI 316L SS at 450ºC by Tsujikawa et al. [28] (mm)			
Nitriding Hour	Measured thickness	Calculated Thickness (γ'+ε)	|Δ Thickness|
8	0.0165	0.0242	**0.0077**

Based on the table 4.13.2 above, the largest difference in thickness between the measured and calculated nitrided thickness was calculated to be at 0.0077 mm which is very small indicating that the mathematical model manage to predict the nitrided layer thickness of the plasma nitrided layer thickness of AISI 316L SS up to great accuracy.

CHAPTER 5: CONCLUSION & RECOMMENDATION

5.1 Conclusion

As mentioned earlier, for the gas nitrided AISI 316L SS, the large difference in thickness between the measured and calculated nitrided thickness was calculated to be the largest at 0.037 mm while the others were in the range of 0.015 to 0.019 mm which accounts for 4/11 of the total possible points. Therefore, this shows that the mathematical model managed to predict the nitrided layer thickness for low temperature gas nitrided AISI 316L SS fairly given by the facts that the other 7/11 other readings indicates that the mathematical model managed to accurately predict the gas nitrided layer thickness of AISI 316L SS.

On the other hand, for low temperature plasma nitrided AISI 316L SS, the largest difference in thickness between the measured and calculated nitrided thickness was calculated to be at 0.0077 mm which is relatively very small indicating that the mathematical model managed to predict the nitrided layer thickness of the plasma nitrided layer thickness of AISI 316L SS up to great accuracy.

In conclusion, the mathematical model managed to accurately predict the plasma nitrided layer thickness of AISI 316L SS which was shown in the table 4.13.2 and also managed to fairly predict the gas nitrided layer thickness of AISI 316L SS which was shown in table 4.13.1.

5.2 Recommendation

The author recommend that the mathematical model is tested for other type of austenitic stainless steel in the 200 and 300 series. This is important in order to determine the range of material in which the mathematical model would works.

Second on the recommendation list is to test the mathematical model for high temperature gas and plasma nitriding of the austenitic stainless steel. The author has not being able to test the model for high temperature application due to the limited time factor and other constrains. The possibility of totally different diffusion mechanism at high temperature might change the whole equation in totality. The mathematical model should follow the diffusion mechanism at high temperature because if the mechanism is different, the mathematical model that the author had proposed would have not been applicable and would not work.

In conclusion, the author would recommend that the mathematical model is tested against other type of low temperature nitrided austenitic stainless steels and also tested for high temperature application. For other type of low temperature nitrided austenitic stainless steel, the mathematical model might not be as accurate as per the case in AISI 316L SS, however, the author would suggest a correlation factors to be introduced to the equation in order to increase the equation accuracy as what Hosseini et al done, by introducing a correlation factor of Kε and Kγ' for the gas and plasma nitriding of the pure iron. Similar methodology should be applicable for the mathematical model reaction with respect to different type of austenitic stainless steels. This correlation of course is must obtained experimentally. Meanwhile, for the application of the mathematical model to high temperature nitriding, the model might not work due to the difference in the diffusion mechanism, therefore, different mathematical model might been necessary to be able to predict the nitrided layer thickness.

REFERENCES

[1]Shaikh, H, Sivaibharasi, N, Sasi, B, Anita, T, Amirthalingam, R, Tao, BPC, Jayakumar, T, Khatak, HS, Raj, B: Use of eddy current testing method in detection and evaluation of sensitazation and intergranular corrosion in austenitic stainless steels. Corros. Sci, 2006, Vol. 48, pg 1462-1482.

[2] Singh, R, Ghowdhury, SG, Ravi Kumar, B, Das, SK, De, PK, Chattoraj, I: The importance of grain size relative to grain boundary character on the sensitization of metastable austenitic stainless steel. Scripta Mater, 2007, Vol. 57, pg. 185–188.

[3] 2008 ASM International, Stainless Steels for Design Engineers.

[4] T. Kumar, P. Jambulingam, M. Gopal, and A. Rajadurai, " Surface Hardening of AISI 304,316,304L and 316L SS using Cyanide Free Salt Bath Nitriding Process", International Symposium of Research Students on Material Science and Engineering 2, 2004.

[5] J. Baranowska," Microstructure Changes in the Upper Surface of Austenitic Steel Induced by Ion Sputtering and Gas Nitriding", Elsevier Applied Surface Science, 2007.

[6] J. Dos Santos, "Improvement of Cavitations Erosion Resistance of a 304L Austenitic Stainless Steel by High Temperature Gas Nitriding", Elsevier Applied Surface Science, 2004.

[7] M. Hassani-Gangaraj, and M. Gualiano, "Microstructure Evolution during Nitriding, Finite Element Simulation and Experimental Assessment", Elsevier Applied Surface Science, 2013.

[8] D.Q. Peng, T.H. Kim, J.H. Chung and J.K. Park, "Development of Nitride-layer of AISI 304 Austenitic Stainless Steel during High-Temperature Ammonia Gas Nitriding", Elsevier Applied Surface Science, 2010.

[9] T. Bell, and K. Akamatsu, Stainless Steels, "Thermomechanical Surface Engineering Stainless Steel" edited by School of Metallurgy & Materials, University of Birmingham, UK, 2010.

[10] M. Yang, "Nitriding- Fundamentals, Modelling and Process Optimization", PhD dissertation, Material Science and Engineering, Worcester Polytechnic Institute, 2012.

[11] UTP Final Year Project Guidelines for Supervisors and Students (2012), version 4.0, pp.30-31.

[12] Scientific Principles, Mechanical Properties [online]. Available: http://matse1.matse.illinois.edu/ceramics/prin.html

[13] Y. Sun and T. Bell: Mater. Sci. Eng. A, 1997, A224, 33-47.

[14] R.E. Schacherl, P.C.J. Graat and E.J. Mittemeijer: Metall. Mater. Trans. A, 2004, 35A, 3387-3398.

[15] J.D. Kammingga and G.C.A.M. Janssen : Surface Coating Technology, 2006, 200, 5896-5901.

[16] J.Crank: 'The mathematics of diffusion'; 1956, Oxford University Press.

[17] M.A.J. Somers, & E.J. Mittemeijer , Layer growth kinetics on gaseous nitriding of pure iron: evaluation of diffusion coefficients for nitrogen in iron nitrides, Metallurgical and Materials Transactions A, vol. 28, pp.57-74, 1995.

[18] H. Du & J.Agren, Theoretical treatment of nitriding and nitrocarburizating of iron, Metallurgical and Material Transaction A, Vol. 27, pp.1073-1080, 1996.

[19] L. Torchane, P. Bilger, J. Dulcy & M. Guntois, "control of iron nitride layers growth kinetics in the binary Fe-N System, Metallurgical and Materials Transactions A, Vol.27, pp. 1823-1835, 1996.

[20] L. Maldzinski, W.Liliental,G. Tymowski & J. Tacikowski, New possibilities for controlling gas nitriding process by simulation of growth kinetics of nitride layers, Surface engineering, Vol.15, pp.377-384, 1999.

[21] M. Keddam, M.E. Djeghlal & L. Barrallier, Computer simulation of nitrided layers growth for pure iron, Comp. Mat. Sci., Vol.29, pp. 43-48, 2004.

[22] M. Keddam, M.E. Djeghlal, & L. Barrallier, a diffusion model for simulation of bilayer growth (ε/γ') of nitrided pure iron, Mat.Sci and Eng. A, Vol.378, pp.475-478, 2004.

[23] S.R. Hosseini, A. Kermanpur & F. Ashrafizadeh, Mathematical modelling of nitrogen depth profile in the nitriding of pure iron, Proc. 8th conference surface engineering and heat treatment, Iranian society of surface science & technology., kerman, pp. 574-578, 2007.

[24] P. Hussain, “diffusion of sialon and stainless steel”, doctoral dissertation, Dept. mechanical engineering, University of Strathclyde, United Kingdom, 1997.

[25] K. Subramaniam and N.T. Ansari, “Surface hardening of 316 LN grade austenitic stainless steel using gas nitriding process”, thesis for bachelor in engineering, S.R.M Engineering College, Kattankulathur, Anna University, Chennai, India, 2006.

[26] N. Renevier. P. Collignon, H. Michel, T. Czerwiec, “Low temperature nitriding of AISI 316L stainless steel and titanium in a low pressure arc discharge”, Surface and Coatings Technology, Vol.11, pp.128-133, 1999.

[27] A. Fossati, F. Borgioli, E. Galvanetto, T. Bacci, “Glow-discharge nitriding of AISI 316L austenitic stainless steel: influence of treatment time”, Surface & Coatings Technology, Vol.200, pp.3511-3517, 2006.

[28] M. Tsujikawa, D. Yoshida, N. Yamauchi, N. Ueda, T. Sone, and S.Tanaka, “ Surface material design of 316 Stainless steel by combination of low temperature carburizing and nitriding”, Surface & Coatings Technology, Vol.200, pp.507-511, 2005.